

Formulation and System Identification of the Equations of Motion for a Dynamic Wind Tunnel Facility

S. D. Carnduff and A. K. Cooke
School of Engineering
Cranfield University
Cranfield
Bedford MK43 0AL
s.d.carnduff@cranfield.ac.uk

The opinions expressed herein are those of the author alone and do not necessarily represent
those of the University

© Cranfield University 2008. All rights reserved. No part of this publication may be reproduced
without the permission of the copyright holder

Formulation and System Identification of the Equations of Motion for a Dynamic Wind Tunnel Facility

College of Aeronautics Report 0801

This document describes the equations of motion of an aircraft model tested in Cranfield's 4 degree-of-freedom (DoF) wind tunnel facility. In previous research, the equations have been derived assuming that the model's centre of gravity (cg) is coincident with the gimbal mechanism about which the model rotates on the rig. However, in this report a general approach is taken with the cg assumed to be located away from the gimbal. The equations are developed from first principles and reduced to a linearised form where motion can be represented as small perturbations about trim. The equations are also decoupled into longitudinal and lateral/direction expressions and converted into state space form. It had been found in practice that models tested in the facility are very responsive in heave and can only be operated open-loop if movement is restricted to purely rotational motion. Therefore, the equations for this 3DoF case are also developed. Having obtained theoretical expressions, a series of wind tunnel tests were conducted on a 1/12 scale BAe Hawk model in order to establish if the theoretical relations were valid in practice. The particular technique used in testing the model was dynamic simulation and the analysis of the experimental data was performed using system identification. An established model structure determination procedure is used to determine which stability and control derivatives should be included in the equations of motion. Frequency domain, equation error parameter estimation is then employed to obtain numerical values for the stability and control derivatives. For both the longitudinal and lateral/directional examples described, the final model structure obtained from experiment matches that derived from theory. Derivatives values obtained from parameter estimation and empirical analysis are also in good agreement.

Contents

Notation	7
1 Introduction	9
2 Axes Systems	11
3 Motion Variables	11
4 Development of the Equations of Moments	12
4.1 Absolute Acceleration Components	12
4.2 Generalised Force Equations	13
4.3 Generalised Moment Equations	14
4.4 Linearised Equations of Motion	15
4.5 Disturbance Forces and Moments	16
4.5.1 Gravitational Terms	17
4.5.2 Aerodynamic and Control Terms	18
4.5.3 Rig Terms	18
4.6 Simplification of Equations	20
4.6.1 Gravitational Terms	21
4.6.2 Aerodynamic and Control Terms	21
4.6.3 Rig Terms	21
4.7 Equations for 3DoF Case	23
4.8 State Space Representation	24
5 Experimental Analysis of 1/12 Scale BAe Hawk Data	25
5.1 Longitudinal Example	32
5.2 Lateral/Directional Example	34
5.3 Comments on the Experimental Results	37
6 Conclusions	38
References	41
A Definition of Concise Derivatives	43
A.1 Longitudinal Derivatives	43
A.1.1 4DoF Case	43
A.1.2 3DoF Case	43
A.2 Lateral/Directional Derivatives	44

List of Figures

1	4DoF rig with 1/12 scale BAe Hawk	9
2	Gimbal mechanism	10
3	Degrees-of-freedom on 4DoF rig	10
4	Motion variables, forces and moments with respect to body-axes origin	12
5	Gravitational forces and moments at trim	17
6	Forces balanced by the rig	19
7	MEMS IMU and miniature servo-actuator	26
8	Illustration of system identification	26
9	Block diagram of system identification process	27
10	Transmission and logging of data	28
11	Fourier sine series coefficients of the angle of attack signal against frequency	29
12	Comparison of measured and identified responses for final model structure	34
13	Comparison of measured and identified responses for final model structure	39

List of Tables

4	Empirical estimates of derivatives	33
5	Initial parameter estimates	33
6	Parameter estimates - z_w dropped	33
7	Parameter estimates - z_η dropped	34
8	Empirical estimates of derivatives	35
9	Initial parameter estimates	36
10	Parameter estimates - y_ζ dropped	36
11	Parameter estimates - l_r dropped	36
12	Parameter estimates - l_ζ dropped	36
13	Parameter estimates - l_p dropped	37
14	Parameter estimates - l_v dropped (p set as a pseudo input)	37
15	Parameter estimates - y_p dropped	38
16	Parameter estimates - y_v dropped	38
17	Confidence ellipsoid elements for n_p dropped	38
18	Parameter estimates - n_p dropped	39

Notation

A	State matrix
B	Input matrix
b_x	State bias term
b_y	Observation bias term
C	Output matrix
D	Direct matrix
<i>D</i>	Direction cosine matrix element
F	Atmospheric turbulence distribution matrix
G	Measurement noise distribution matrix
<i>g</i>	Acceleration due to gravity
<i>I_{xx}</i>	Moment of inertia in roll
<i>I_{yy}</i>	Moment of inertia in pitch
<i>I_{zz}</i>	Moment of inertia in yaw
<i>I_{xy}</i>	Product of inertia about <i>x</i> and <i>y</i> axes
<i>I_{xz}</i>	Product of inertia about <i>x</i> and <i>z</i> axes
<i>I_{yz}</i>	Product of inertia about <i>y</i> and <i>z</i> axes
L	Rolling moment
M	Pitching moment
<i>m</i>	Model/aircraft mass
N	Yawing moment
<i>N</i>	Number of discrete measurement points in time
<i>n_u</i>	Number of control surface input variables
<i>n_x</i>	Number of state variables
<i>n_y</i>	Number of observation variables
<i>P</i>	Roll rate variable
<i>P_e</i>	Roll rate variable at trim
<i>p</i>	Roll rate perturbation variable and arbitrary point on aircraft model
<i>Q</i>	Pitch rate variable
<i>Q_e</i>	Pitch rate variable at trim
<i>q</i>	Pitch rate perturbation variable
<i>R</i>	Yaw rate variable
<i>R_e</i>	Yaw rate variable at trim
<i>r</i>	Yaw rate perturbation variable
<i>t</i>	Time
<i>U</i>	Axial velocity variable
<i>U_e</i>	Axial velocity variable at trim
u	Control input vector
<i>V</i>	Sideslip velocity variable
<i>V_e</i>	Axial velocity variable at trim
<i>V_T</i>	Wind tunnel velocity vector
<i>v</i>	Sideslip velocity perturbation variable
v	Measurement noise vector
<i>v</i>	Sideslip velocity perturbation variable
<i>W</i>	Heave velocity in body axes
<i>W_e</i>	Heave velocity in body axes at trim
<i>W_{rig}</i>	Heave velocity in rig axes
<i>W_{rig_e}</i>	Heave velocity in rig axes at trim
w	Process noise vector
<i>w</i>	Heave velocity perturbation variable

X	Axial force
\mathbf{x}	State variable vector
x	Longitudinal coordinate in axis system
Y	Lateral force
\mathbf{y}	Observation vector
y	Lateral coordinate in axis system
Z	Normal force
\mathbf{z}	Measurement vector
z	Normal coordinate in axis system

Greek Letters

ζ	Rudder input
η	Elevator input
Θ	Pitch attitude variable
Θ_e	Pitch attitude variable at trim
θ	Pitch attitude perturbation variable
λ	Geometric scale factor between scale model and full-sized aircraft
ξ	Aileron input
ρ	Atmospheric density
Φ	Roll attitude variable
Φ_e	Roll attitude variable at trim
ϕ	Roll attitude perturbation variable
Ψ	Yaw attitude variable
Ψ_e	Yaw attitude variable at trim
ψ	Yaw attitude perturbation variable

Subscripts

0	Initial condition
a	Aerodynamic force or moment
b	Aircraft model body axes
c	Control force or moment
e	Equilibrium/trim condition
g	Coordinates of cg relative to body axes origin and gravitational force or moment
rig	Rig axes and rig force

1 Introduction

The dynamic wind tunnel facility at Cranfield University was originally developed in the early 1980s [1, 2] and has been used to investigate a number of aircraft configurations [3, 4]. Figure 1 shows the test rig with a 1/12 scale model of the BAe Hawk, which has been used as a platform for testing the facility's instrumentation and hardware. The design of the rig is relatively simple, with the aircraft model suspended on a stiff vertical rod, which is itself attached to a Dexion framework. The vertical rod passes through a gimbal mechanism within the model, shown in Figure 2, that allows the aircraft to rotate in roll, pitch and yaw and to translate vertically along the axis of the rod. The rig therefore allows investigation of 4 degrees of freedom (DoF) of motion (see Figure 3). The range of motion that the rig permits is ± 30 degrees rotation in roll and pitch, 360 degrees in yaw and a translation of approximately 0.75m in the vertical axis. The gimbal and rod assembly was made as small and as light as possible to minimise their influence on the aircraft model and the gimbal incorporates precision ballraces and linear ball bearings to minimize frictional effects. The test rig is designed to be placed in an open section wind tunnel. The facility currently being used has a working section of 1.5m by 1.1m and a maximum speed of 40m/s inside the working section. The maximum wing span of the model is limited to around 0.9m.



Figure 1: 4DoF rig with 1/12 scale BAe Hawk

In earlier work, the equations of motions of a model in the facility had been derived assuming that the model's centre of gravity (cg) was coincident with the gimbal mechanism. However, this may not be true in practice, so in this report the equations are developed for the case where the model cg is located away from the gimbal. It is assumed throughout this report that the model being tested has been appropriately scaled according to similarity and dynamic scaling laws. The issues of dynamic scaling and similarity are not discussed here but detailed descriptions can be found in a number of texts [1, 3, 5, 6]. The effects of friction between the gimbal mechanism and the rod are also assumed to be negligible in the development of the equations.

Having developed the equations of motion from first principles, an aim of the current research was to

carry out an experimental analysis to confirm that these relationships were valid in practice. Therefore, a series of wind tunnel tests were carried out on the 1/12 scale BAe Hawk model, shown in Figure 1. The approach used in the tests is known as dynamic simulation [1, 3, 4, 7, 8, 9, 10, 11]. In this case, a dynamically-scaled model with representative control surfaces is mounted on the test rig and flown in semi-free flight. Specific inputs are applied to the control surfaces, which are deflected using miniature servo-actuators, and the resultant response of the model is measured using motion sensors. The stability and control derivatives can then be extracted from the input/output data using system identification and parameter estimation techniques similar to those used in the flight test environment.

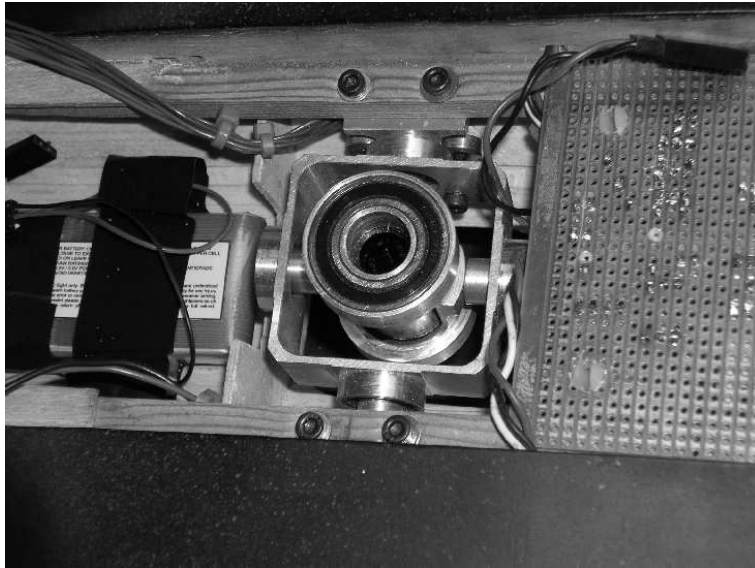


Figure 2: Gimbal mechanism

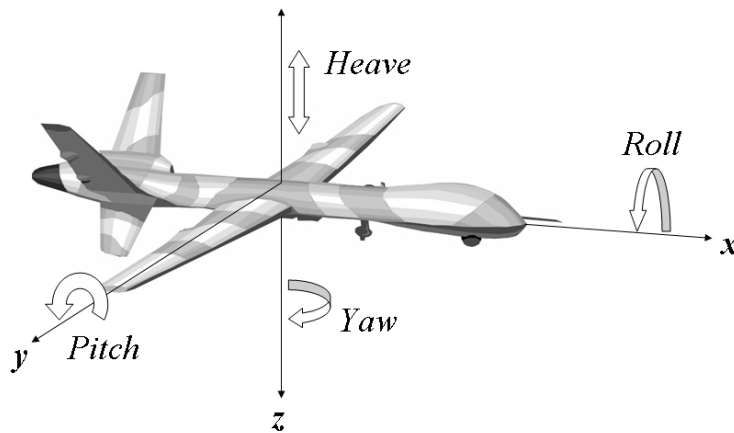


Figure 3: Degrees-of-freedom on 4DoF rig

The following section describes the axes systems used throughout this report, while Section 3 defines the model motion variables. The equations of motion are then derived from first principles in Section 4. A general approach is taken at first before some simplifying assumptions are outlined. The equations are decoupled into linearised longitudinal and lateral/directional sets of expressions, which in turn allows the equations to be written in state space form. Experimental analysis of the 1/12 scale BAe Hawk is described in Section 5. This includes a brief description of system identification as applied to aircraft, the specific techniques used in the analysis for this report, and a comparison between the theoretical and experimental results. The report is brought to a close with some conclusions in Section 6.

2 Axes Systems

In the development of the equations of motion, two axes systems will be defined, both with origins initially co-located at the gimbal:

- Rig axes: x_{rig} points into the tunnel and is assumed to be aligned with the tunnel velocity vector V_T which is assumed to be parallel to the ground, y_{rig} is normal to V_T and also parallel to the ground, and z_{rig} points vertically down.
- Body axes: x_b points along the nose of the aircraft model and is assumed to be aligned with the horizontal fuselage datum, y_b is normal to x_b and points starboard, and z_b points down through the underside of the aircraft model.

Rig axes are fixed in inertial space, while the body axes rotate and translate with the aircraft model, which moves relative to the airflow from the tunnel.

3 Motion Variables

As illustrated in Figure 3, the rig constrains motion along the x_{rig} and y_{rig} axes but allows the model to translate along z_{rig} . Rotational motion is allowed about all three axes. When motion is referenced to the rig axes, the model moves relative to the airflow with an axial velocity equal to the tunnel speed V_T and a heave velocity denoted W_{rig} . The angular rates about x_{rig} , y_{rig} and z_{rig} are given by P_{rig} , Q_{rig} and R_{rig} respectively. In body axes, the translational velocity components along x_b , y_b and z_b are given by U , V and W respectively, while the roll, pitch and yaw rates about the same axes are denoted P , Q and R .

For disturbed motion, with the aircraft model rolled, pitched and yawed through angles Φ , Θ and Ψ , the translational velocities in rig axes are transformed into body axes using the equation,

$$\begin{bmatrix} U \\ V \\ W \end{bmatrix} = \begin{bmatrix} D_{11} & D_{12} & D_{13} \\ D_{21} & D_{22} & D_{23} \\ D_{31} & D_{32} & D_{33} \end{bmatrix} \begin{bmatrix} V_T \\ 0 \\ W_{rig} \end{bmatrix} \quad (3.1)$$

where

$$\begin{aligned} D_{11} &= \cos \Theta \cos \Psi \\ D_{12} &= \cos \Theta \sin \Psi \\ D_{13} &= -\sin \Theta \\ D_{21} &= \sin \Phi \sin \Theta \cos \Psi - \cos \Phi \sin \Psi \\ D_{22} &= \sin \Phi \sin \Theta \sin \Psi + \cos \Phi \cos \Psi \\ D_{23} &= \sin \Phi \cos \Theta \\ D_{31} &= \cos \Phi \sin \Theta \cos \Psi + \sin \Phi \sin \Psi \\ D_{32} &= \cos \Phi \sin \Theta \sin \Psi - \sin \Phi \cos \Psi \\ D_{33} &= \cos \Phi \cos \Theta \end{aligned} \quad (3.2)$$

Therefore,

$$\begin{bmatrix} U \\ V \\ W \end{bmatrix} = \begin{bmatrix} D_{11}V_T + D_{13}W_{rig} \\ D_{21}V_T + D_{23}W_{rig} \\ D_{31}V_T + D_{33}W_{rig} \end{bmatrix} \quad (3.3)$$

Angular rates are transformed in a similar manner,

$$\begin{bmatrix} P \\ Q \\ R \end{bmatrix} = \begin{bmatrix} D_{11}P_{rig} + D_{12}Q_{rig} + D_{13}R_{rig} \\ D_{21}P_{rig} + D_{22}Q_{rig} + D_{23}R_{rig} \\ D_{31}P_{rig} + D_{32}Q_{rig} + D_{33}R_{rig} \end{bmatrix} \quad (3.4)$$

It is also worth noting that as the wind tunnel velocity vector V_T is assumed to act parallel to the ground, the model's angle of attack α and pitch angle Θ are the same.

4 Development of the Equations of Moments

In this section, the equations of motion for a model on the rig are developed from first principles using a method similar to that used to derive the equations of motion for a free-flying aircraft.

4.1 Absolute Acceleration Components

A point p is arbitrarily chosen within the aircraft model, with coordinates (x, y, z) with respect to the origin. The local components of velocity and acceleration of p relative to the origin are denoted u, v, w and a_x, a_y, a_z . As already mentioned in the introduction, it is assumed that the origin of the body axes and the cg of the model are not coincident, with the cg having coordinates (x_g, y_g, z_g) . See Figure 4.

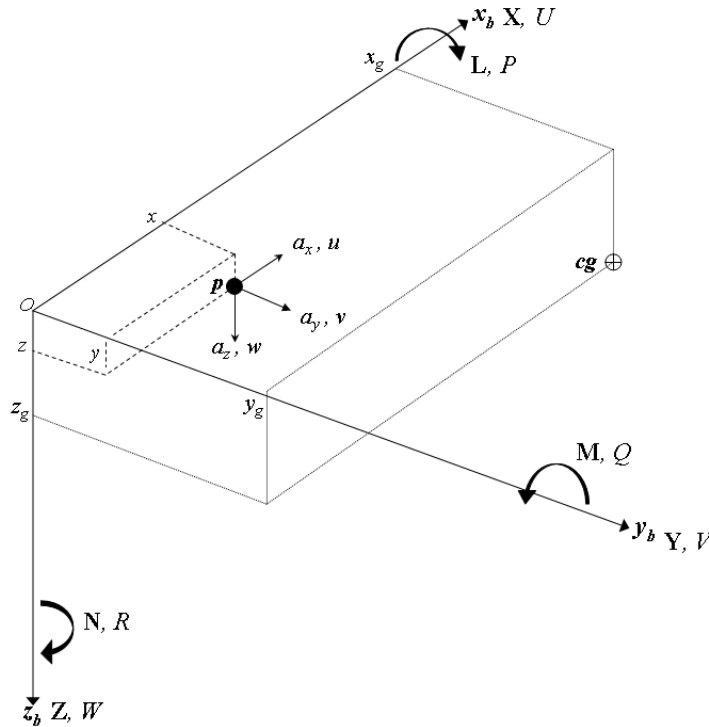


Figure 4: Motion variables, forces and moments with respect to body-axes origin

The velocity components of p relative to the origin are,

$$\begin{bmatrix} u \\ v \\ w \end{bmatrix} = \begin{bmatrix} \dot{x} - Ry + Qz \\ \dot{y} - Pz + Rx \\ \dot{z} - Qx + Py \end{bmatrix} \quad (4.1)$$

If the aircraft model is assumed to be rigid $\dot{x} = \dot{y} = \dot{z} = 0$ then,

$$\begin{bmatrix} u \\ v \\ w \end{bmatrix} = \begin{bmatrix} -Ry + Qz \\ -Pz + Rx \\ -Qx + Py \end{bmatrix} \quad (4.2)$$

The acceleration components of p relative to the origin are given by,

$$\begin{bmatrix} a_x \\ a_y \\ a_z \end{bmatrix} = \begin{bmatrix} \dot{u} - Rv + Qw \\ \dot{v} - Pw + Ru \\ \dot{w} - Qu + Pv \end{bmatrix} \quad (4.3)$$

By superimposing the velocity components at the origin onto the local velocity components, the absolute velocity components at p are obtained,

$$\begin{bmatrix} u' \\ v' \\ w' \end{bmatrix} = \begin{bmatrix} U + u \\ V + v \\ W + w \end{bmatrix} = \begin{bmatrix} U - Ry + Qz \\ V - Pz + Rx \\ W - Qx + Py \end{bmatrix} \quad (4.4)$$

Similarly, the absolute acceleration components at p are given by,

$$\begin{bmatrix} a'_x \\ a'_y \\ a'_z \end{bmatrix} = \begin{bmatrix} \dot{u}' - Rv' + Qw' \\ \dot{v}' - Pw' + Ru' \\ \dot{w}' - Qu' + Pv' \end{bmatrix} \quad (4.5)$$

Differentiating (4.4) with respect to time and again assuming a rigid body,

$$\begin{bmatrix} \dot{u}' \\ \dot{v}' \\ \dot{w}' \end{bmatrix} = \begin{bmatrix} \dot{U} - \dot{R}y + \dot{Q}z \\ \dot{V} - \dot{P}z + \dot{R}x \\ \dot{W} - \dot{Q}x + \dot{P}y \end{bmatrix} \quad (4.6)$$

Substituting (4.4) and (4.6) into (4.5), the expressions for absolute acceleration components of p become,

$$\begin{bmatrix} a'_x \\ a'_y \\ a'_z \end{bmatrix} = \begin{bmatrix} \dot{U} - RV + QW - x(Q^2 + R^2) + y(PQ - \dot{R}) + z(\dot{Q} + PR) \\ \dot{V} - PW + RU + x(PQ + \dot{R}) - y(P^2 + R^2) + z(QR - \dot{P}) \\ \dot{W} - QU + PV + x(PR - \dot{Q}) + y(QR + \dot{P}) - z(P^2 + Q^2) \end{bmatrix} \quad (4.7)$$

4.2 Generalised Force Equations

Consider an incremental mass δm at point p . Applying Newton's Second Law, the incremental components of force acting on the mass are given by $\delta m a'_x$, $\delta m a'_y$ and $\delta m a'_z$. The total force components acting at the origin are given by summing the force increments over the entire body,

$$\begin{bmatrix} \sum \delta m a'_x \\ \sum \delta m a'_y \\ \sum \delta m a'_z \end{bmatrix} = \begin{bmatrix} X \\ Y \\ Z \end{bmatrix} \quad (4.8)$$

where a'_x , a'_y and a'_z are the absolute acceleration components at the cg of the model. So, using (4.7), the resultant force components acting at the body axes centre are given by,

$$\begin{bmatrix} X \\ Y \\ Z \end{bmatrix} = m \begin{bmatrix} \dot{U} - RV + QW - x_g(Q^2 + R^2) + y_g(PQ - \dot{R}) + z_g(\dot{Q} + PR) \\ \dot{V} - PW + RU + x_g(PQ + \dot{R}) - y_g(P^2 + R^2) + z_g(QR - \dot{P}) \\ \dot{W} - QU + PV + x_g(PR - \dot{Q}) + y_g(QR + \dot{P}) - z_g(P^2 + Q^2) \end{bmatrix} \quad (4.9)$$

where m is the total mass of the model.

4.3 Generalised Moment Equations

Consider the moments produced by the force acting on the incremental mass δm at p ,

$$\begin{bmatrix} \mathbf{L} \\ \mathbf{M} \\ \mathbf{N} \end{bmatrix} = \begin{bmatrix} \sum \delta m (y a'_z - z a'_y) \\ \sum \delta m (z a'_x - x a'_z) \\ \sum \delta m (x a'_y - y a'_x) \end{bmatrix} \quad (4.10)$$

where L, M and N are the rolling, pitching and yawing moments respectively. Considering the rolling moment equation in isolation, expressions for a'_z and a'_y from Equation (4.7) can be inserted into (4.10) to give, after some rearrangement,

$$\begin{aligned} \mathbf{L} = & \sum \delta m y (\dot{W} - QU + PV) - \sum \delta m z (\dot{V} - PW + RU) + \sum \delta m xy (PR - \dot{Q}) \\ & + \dot{P} \sum \delta m (y^2 + z^2) + QR \sum \delta m (y^2 - z^2) + \sum \delta m yz (R^2 - Q^2) - \sum \delta m xz (PQ + \dot{R}) \end{aligned} \quad (4.11)$$

The summation terms in Equation (4.11) represent the moments and products of inertia about the body axes centre and are defined as follows:

$$\begin{aligned} [I_{xx}]_b &= \sum (y^2 + z^2) \delta m - \text{Moment of Inertia about } x_b \\ [I_{yy}]_b &= \sum (x^2 + z^2) \delta m - \text{Moment of Inertia about } y_b \\ [I_{zz}]_b &= \sum (x^2 + y^2) \delta m - \text{Moment of Inertia about } z_b \\ [I_{xy}]_b &= \sum xy \delta m - \text{Product of Inertia about } x_b \text{ and } y_b \\ [I_{yz}]_b &= \sum yz \delta m - \text{Product of Inertia about } y_b \text{ and } z_b \\ [I_{xz}]_b &= \sum xz \delta m - \text{Product of Inertia about } x_b \text{ and } z_b \end{aligned}$$

Note that $\sum (y^2 - z^2) \delta m = \sum (x^2 + y^2) \delta m - \sum (x^2 + z^2) \delta m = [I_{zz}]_b - [I_{yy}]_b$. Therefore the rolling moment equation becomes:

$$\begin{aligned} \mathbf{L} = & m y (\dot{W} - QU + PV) - m z (\dot{V} - PW + RU) + [I_{xx}]_b \dot{P} + [I_{xy}]_b (PR - \dot{Q}) \\ & + ([I_{zz}]_b - [I_{yy}]_b) QR + [I_{yz}]_b (R^2 - Q^2) - [I_{xz}]_b (PQ + \dot{R}) \end{aligned} \quad (4.12)$$

It may be that the inertia properties of the model are known about an axis system with an origin located at the cg rather than the body axes centre. If this is the case, information about the moments and products of inertia about the body axes centre can be obtained to using parallel axis theorem,

$$[I_{xx}]_b = I_{xx} + m(y_g^2 + z_g^2) \quad (4.13)$$

$$[I_{yy}]_b = I_{yy} + m(x_g^2 + z_g^2) \quad (4.14)$$

$$[I_{zz}]_b = I_{zz} + m(x_g^2 + y_g^2) \quad (4.15)$$

$$[I_{xy}]_b = I_{xy} + m x_g y_g \quad (4.16)$$

$$[I_{yz}]_b = I_{yz} + m y_g z_g \quad (4.17)$$

$$[I_{xz}]_b = I_{xz} + m x_g z_g \quad (4.18)$$

where I_{xx} , I_{yy} , I_{zz} , I_{xy} , I_{yz} and I_{xz} are the moments and products of inertia about the model cg and x_g , y_g and z_g are again used to denote the offsets of the cg from the body axes origin. Note that it has been assumed that there is no angular misalignment between the body axes and axis system at the cg about which the inertia properties are referenced.

Utilising the above expressions for the inertias and the generalised force equations in (4.9), the rolling moment equation can be rearranged to give,

$$\mathbf{L} = I_{xx} \dot{P} + (I_{zz} - I_{yy}) QR - I_{xz} (PQ + \dot{R}) - Y z_g \quad (4.19)$$

In a similar manner, expressions for the pitching and yawing moments can be developed,

$$M = I_{yy}\dot{Q} - (I_{xx} - I_{zz})PR - I_{xz}(R^2 - P^2) + Xz_g - Zx_g \quad (4.20)$$

$$N = I_{zz}\dot{R} + (I_{yy} - I_{xx})PQ + I_{xz}(QR - \dot{P}) + Yx_g \quad (4.21)$$

Hence Equations (4.19) to (4.21) are expressions for the rolling, pitching and yawing moments about the body axes origin with the inertias referenced to the cg. Note also that the terms involving I_{xy} and I_{yz} have been neglected. It is assumed the aircraft model is symmetric about the xz -plane, with the mass evenly distributed. Therefore $I_{xy} = I_{yz} = 0$. For the same reason, the lateral offset y_g between the origin of the reference axes and the cg will be zero for a symmetric model.

4.4 Linearised Equations of Motion

At trim, it is assumed that the model is not moving relative to the rig and is undergoing no angular motion. That is,

$$W_{rig_e} = P_{rig_e} = Q_{rig_e} = R_{rig_e} = P_e = Q_e = R_e = 0$$

where the subscript e denotes trim conditions. For the most general of cases, the trimmed roll, pitch and yaw angles of the model relative to the rig are denoted Φ_e , Θ_e and Ψ_e . Using Equation (3.3), the trimmed body axes velocity components can be related to the trimmed rig axes velocity components by,

$$\begin{bmatrix} U_e \\ V_e \\ W_e \end{bmatrix} = \begin{bmatrix} D_{11e} & D_{12e} & D_{13e} \\ D_{21e} & D_{22e} & D_{23e} \\ D_{31e} & D_{32e} & D_{33e} \end{bmatrix} \begin{bmatrix} V_T \\ 0 \\ 0 \end{bmatrix} = \begin{bmatrix} D_{11e} V_T \\ D_{21e} V_T \\ D_{31e} V_T \end{bmatrix} \quad (4.22)$$

The definitions of the direction cosine matrix elements are the same as those given in (3.2) with Φ , Θ and Ψ replaced by the trim angles Φ_e , Θ_e and Ψ_e respectively.

If now the model experiences a small disturbance about trim, the resulting perturbation in vertical velocity in rig axes is denoted w_{rig} , while roll, pitch and yaw rate perturbations about the same axis system are given by p_{rig} , q_{rig} and r_{rig} respectively. The resulting roll, pitch and yaw attitudes due to the disturbance are ϕ , θ and ψ . The tunnel speed V_T is assumed to remain constant.

So, the translational velocity components in body axes generated by the disturbance are found from (3.3),

$$\begin{bmatrix} U \\ V \\ W \end{bmatrix} = \begin{bmatrix} U_e + u \\ V_e + v \\ W_e + w \end{bmatrix} = \begin{bmatrix} D_{11}V_T + D_{13}w_{rig} \\ D_{21}V_T + D_{23}w_{rig} \\ D_{31}V_T + D_{33}w_{rig} \end{bmatrix} \quad (4.23)$$

where u , v and w denote perturbations in the velocity components U , V and W . Similarly, the angular rates components in body axes are found using (3.4),

$$\begin{bmatrix} P \\ Q \\ R \end{bmatrix} = \begin{bmatrix} P_e + p \\ Q_e + q \\ R_e + r \end{bmatrix} = \begin{bmatrix} p \\ q \\ r \end{bmatrix} = \begin{bmatrix} D_{11}p_{rig} + D_{12}q_{rig} + D_{13}r_{rig} \\ D_{21}p_{rig} + D_{22}q_{rig} + D_{23}r_{rig} \\ D_{31}p_{rig} + D_{32}q_{rig} + D_{33}r_{rig} \end{bmatrix} \quad (4.24)$$

where p , q and r are the angular rate perturbations in body axes. Expressions for the direction cosine elements can now be developed. As an example, the element D_{12} will be considered. Following the perturbation from trim, D_{12} can be written as,

$$D_{12} = \cos(\Theta_e + \theta) \sin(\Psi_e + \psi) \quad (4.25)$$

Equation (4.25) can be expanded by using the trigonometric identities

$$\begin{aligned}\cos(A + B) &= \cos A \cos B - \sin A \sin B \\ \sin(A + B) &= \sin A \cos B + \cos A \sin B\end{aligned}$$

Therefore,

$$D_{12} = (\cos \Theta_e \cos \theta - \sin \Theta_e \sin \theta)(\sin \Psi_e \cos \psi + \cos \Psi_e \sin \psi) \quad (4.26)$$

It is noted that the attitude perturbation ϕ , θ and ψ have small values, hence using small angle theory ,

$$\begin{aligned}\cos \phi &= \cos \theta = \cos \psi \approx 1 \\ \sin \phi &\approx \phi, \quad \sin \theta \approx \theta, \quad \sin \psi \approx \psi\end{aligned}$$

and Equation (4.26) reduces to,

$$D_{12} = C_\theta S_\psi \quad (4.27)$$

where $C_\theta = (\cos \Theta_e - \theta \sin \Theta_e)$ and $S_\psi = (\sin \Psi_e + \psi \cos \Psi_e)$. Using the above approach, the remaining direction cosine terms can be written as follows,

$$\begin{aligned}D_{11} &= C_\theta C_\psi \\ D_{12} &= C_\theta S_\psi \\ D_{13} &= -S_\theta \\ D_{21} &= S_\phi S_\theta C_\psi - C_\phi S_\psi \\ D_{22} &= S_\phi S_\theta S_\psi + C_\phi C_\psi \\ D_{23} &= S_\phi C_\theta \\ D_{31} &= C_\phi S_\theta C_\psi + S_\phi S_\psi \\ D_{32} &= C_\phi S_\theta S_\psi - S_\phi C_\psi \\ D_{33} &= C_\phi C_\theta\end{aligned} \quad (4.28)$$

where $C_k = (\cos k_e - k \sin k_e)$ and $S_k = (\sin k_e + k \cos k_e)$ for $k = \phi, \theta, \psi$.

The small perturbation assumption can also be used to reduce the terms on the left hand side of the generalised force equations in (4.9) and moment equations (4.19) to (4.21). Removing terms that have zero trim values and neglecting products and squares of small perturbation variables, the force and moment equations become,

$$m(\dot{u} - rV_e + qW_e + z_g \dot{q}) = X \quad (4.29)$$

$$m(\dot{v} - pW_e + rU_e + \dot{r}x_g - \dot{p}z_g) = Y \quad (4.30)$$

$$m(\dot{w} - qU_e + pV_e - x_g \dot{q}) = Z \quad (4.31)$$

$$I_{xx} \dot{p} - I_{xz} \dot{r} - mz_g(\dot{v} - pW_e + rU_e + \dot{r}x_g - \dot{p}z_g) = L \quad (4.32)$$

$$I_{yy} \dot{q} + mz_g(\dot{u} - rV_e + qW_e + z_g \dot{q}) - mx_g(\dot{w} - qU_e + pV_e - \dot{q}x_g) = M \quad (4.33)$$

$$I_{zz} \dot{r} - I_{xz} \dot{p} + mx_g(\dot{v} - pW_e + rU_e + \dot{r}x_g - \dot{p}z_g) = N \quad (4.34)$$

Having dealt with the left hand side of the force and moment equations, the terms on the right hand side can now be considered.

4.5 Disturbance Forces and Moments

It is assumed that the disturbing forces and moments on the model are due to aerodynamic effects, gravitational effects and movement of the control surfaces, with the tunnel airflow assumed to be stable. In addition, the force components acting along the x_{rig} and y_{rig} axes will be balanced by reaction forces

from the rig, as motion along these axes is constrained. So, for example, the force and moment components can be written in the form,

$$\begin{aligned} \mathbf{X} &= \mathbf{X}_a + \mathbf{X}_g + \mathbf{X}_c + \mathbf{X}_{rig_b} \\ \mathbf{M} &= \mathbf{M}_a + \mathbf{M}_g + \mathbf{M}_c \end{aligned}$$

where \mathbf{X}_{rig_b} represents the components of the rig reaction forces along x_{rig} and y_{rig} transformed into body axes, acting along x_b .

4.5.1 Gravitational Terms

Figure 5 shows the relationship between the forces and moments acting at the body axes origin at trim and the gravity vector acting at the cg. The following expressions can hence be developed,

$$\begin{bmatrix} \mathbf{X}_{g_e} \\ \mathbf{Y}_{g_e} \\ \mathbf{Z}_{g_e} \end{bmatrix} = \begin{bmatrix} D_{11e} & D_{12e} & D_{13e} \\ D_{21e} & D_{22e} & D_{23e} \\ D_{31e} & D_{32e} & D_{33e} \end{bmatrix} \begin{bmatrix} 0 \\ 0 \\ mg \end{bmatrix} = \begin{bmatrix} -mg \sin \Theta_e \\ mg \sin \Phi_e \cos \Theta_e \\ mg \cos \Phi_e \cos \Theta_e \end{bmatrix} \quad (4.35)$$

$$\begin{bmatrix} \mathbf{L}_{g_e} \\ \mathbf{M}_{g_e} \\ \mathbf{N}_{g_e} \end{bmatrix} = \begin{bmatrix} D_{11e} & D_{12e} & D_{13e} \\ D_{21e} & D_{22e} & D_{23e} \\ D_{31e} & D_{32e} & D_{33e} \end{bmatrix} \begin{bmatrix} 0 \\ -x_g mg \\ 0 \end{bmatrix} = \begin{bmatrix} -x_g mg \cos \Theta_e \sin \Psi_e \\ -x_g mg (\sin \Phi_e \sin \Theta_e \sin \Psi_e + \cos \Phi_e \cos \Psi_e) \\ -x_g mg (\cos \Phi_e \sin \Theta_e \sin \Psi_e - \sin \Phi_e \cos \Psi_e) \end{bmatrix} \quad (4.36)$$

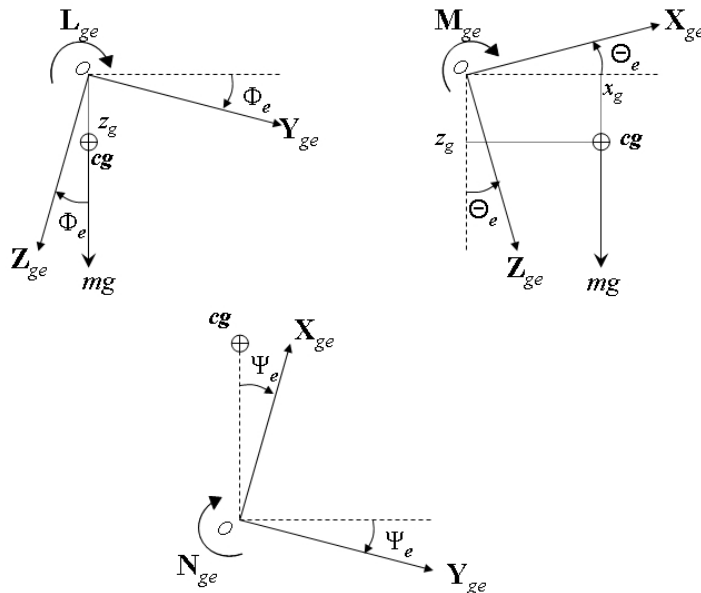


Figure 5: Gravitational forces and moments at trim

For the disturbed case,

$$\begin{bmatrix} \mathbf{X}_g \\ \mathbf{Y}_g \\ \mathbf{Z}_g \end{bmatrix} = \begin{bmatrix} 1 & \psi & -\theta \\ -\psi & 1 & \phi \\ \theta & -\phi & 1 \end{bmatrix} \begin{bmatrix} \mathbf{X}_{g_e} \\ \mathbf{Y}_{g_e} \\ \mathbf{Z}_{g_e} \end{bmatrix} = \begin{bmatrix} -mg \sin \Theta_e + mg\psi \sin \Phi_e \cos \Theta_e - mg\theta \cos \Phi_e \cos \Theta_e \\ mg\psi \sin \Theta_e + mg \sin \Phi_e \cos \Theta_e + mg\phi \cos \Phi_e \cos \Theta_e \\ -mg\theta \sin \Theta_e - mg\phi \sin \Phi_e \cos \Theta_e + mg \cos \Phi_e \cos \Theta_e \end{bmatrix} \quad (4.37)$$

$$\begin{bmatrix} \mathbf{L}_g \\ \mathbf{M}_g \\ \mathbf{N}_g \end{bmatrix} = \begin{bmatrix} 1 & \psi & -\theta \\ -\psi & 1 & \phi \\ \theta & -\phi & 1 \end{bmatrix} \begin{bmatrix} \mathbf{L}_{g_e} \\ \mathbf{M}_{g_e} \\ \mathbf{N}_{g_e} \end{bmatrix} \quad (4.38)$$

so

$$\begin{aligned} \mathbf{L}_g = & -x_g mg \cos \Theta_e \sin \Psi_e - x_g mg \psi (\sin \Phi_e \sin \Theta_e \sin \Psi_e + \cos \Phi_e \cos \Psi_e) \\ & + x_g mg \theta (\cos \Phi_e \sin \Theta_e \sin \Psi_e - \sin \Phi_e \cos \Psi_e) \end{aligned}$$

$$\begin{aligned} \mathbf{M}_g = & x_g mg \psi \cos \Theta_e \sin \Psi_e - x_g mg (\sin \Phi_e \sin \Theta_e \sin \Psi_e + \cos \Phi_e \cos \Psi_e) \\ & - x_g mg \phi (\cos \Phi_e \sin \Theta_e \sin \Psi_e - \sin \Phi_e \cos \Psi_e) \end{aligned}$$

$$\begin{aligned} \mathbf{N}_g = & -x_g mg \theta \cos \Theta_e \sin \Psi_e + x_g mg \phi (\sin \Phi_e \sin \Theta_e \sin \Psi_e + \cos \Phi_e \cos \Psi_e) \\ & - x_g mg (\cos \Phi_e \sin \Theta_e \sin \Psi_e - \sin \Phi_e \cos \Psi_e) \end{aligned}$$

where the following 3×3 matrix is the direction cosine matrix for small perturbations and angles:

$$\begin{bmatrix} 1 & \psi & -\theta \\ -\psi & 1 & \phi \\ \theta & -\phi & 1 \end{bmatrix}$$

4.5.2 Aerodynamic and Control Terms

The aerodynamic and control terms are developed using a Taylor series expansion about the initial conditions for each of the forces and moments in a similar manner to that described by Cook [12]. Only the first term in each series is considered significant and the only higher order derivatives retained are those with respect to \dot{w} .

$$\mathbf{X}_a + \mathbf{X}_c = \mathbf{X}_{a_e} + \dot{\mathbf{X}}_u u + \dot{\mathbf{X}}_v v + \dot{\mathbf{X}}_w w + \dot{\mathbf{X}}_p p + \dot{\mathbf{X}}_q q + \dot{\mathbf{X}}_r r + \dot{\mathbf{X}}_{\dot{w}} \dot{w} + \dot{\mathbf{X}}_{\eta} \eta + \dot{\mathbf{X}}_{\xi} \xi + \dot{\mathbf{X}}_{\zeta} \zeta \quad (4.39)$$

$$\mathbf{Y}_a + \mathbf{Y}_c = \mathbf{Y}_{a_e} + \dot{\mathbf{Y}}_u u + \dot{\mathbf{Y}}_v v + \dot{\mathbf{Y}}_w w + \dot{\mathbf{Y}}_p p + \dot{\mathbf{Y}}_q q + \dot{\mathbf{Y}}_r r + \dot{\mathbf{Y}}_{\dot{w}} \dot{w} + \dot{\mathbf{Y}}_{\eta} \eta + \dot{\mathbf{Y}}_{\xi} \xi + \dot{\mathbf{Y}}_{\zeta} \zeta \quad (4.40)$$

$$\mathbf{Z}_a + \mathbf{Z}_c = \mathbf{Z}_{a_e} + \dot{\mathbf{Z}}_u u + \dot{\mathbf{Z}}_v v + \dot{\mathbf{Z}}_w w + \dot{\mathbf{Z}}_p p + \dot{\mathbf{Z}}_q q + \dot{\mathbf{Z}}_r r + \dot{\mathbf{Z}}_{\dot{w}} \dot{w} + \dot{\mathbf{Z}}_{\eta} \eta + \dot{\mathbf{Z}}_{\xi} \xi + \dot{\mathbf{Z}}_{\zeta} \zeta \quad (4.41)$$

$$\mathbf{L}_a + \mathbf{L}_c = \mathbf{L}_{a_e} + \dot{\mathbf{L}}_u u + \dot{\mathbf{L}}_v v + \dot{\mathbf{L}}_w w + \dot{\mathbf{L}}_p p + \dot{\mathbf{L}}_q q + \dot{\mathbf{L}}_r r + \dot{\mathbf{L}}_{\dot{w}} \dot{w} + \dot{\mathbf{L}}_{\eta} \eta + \dot{\mathbf{L}}_{\xi} \xi + \dot{\mathbf{L}}_{\zeta} \zeta \quad (4.42)$$

$$\begin{aligned} \mathbf{M}_a + \mathbf{M}_c = & \mathbf{M}_{a_e} + \dot{\mathbf{M}}_u u + \dot{\mathbf{M}}_v v + \dot{\mathbf{M}}_w w + \dot{\mathbf{M}}_p p + \dot{\mathbf{M}}_q q + \dot{\mathbf{M}}_r r + \dot{\mathbf{M}}_{\dot{w}} \dot{w} \\ & + \dot{\mathbf{M}}_{\eta} \eta + \dot{\mathbf{M}}_{\xi} \xi + \dot{\mathbf{M}}_{\zeta} \zeta \end{aligned} \quad (4.43)$$

$$\mathbf{N}_a + \mathbf{N}_c = \mathbf{N}_{a_e} + \dot{\mathbf{N}}_u u + \dot{\mathbf{N}}_v v + \dot{\mathbf{N}}_w w + \dot{\mathbf{N}}_p p + \dot{\mathbf{N}}_q q + \dot{\mathbf{N}}_r r + \dot{\mathbf{N}}_{\dot{w}} \dot{w} + \dot{\mathbf{N}}_{\eta} \eta + \dot{\mathbf{N}}_{\xi} \xi + \dot{\mathbf{N}}_{\zeta} \zeta \quad (4.44)$$

Note the control terms η , ξ and ζ represent inputs about the values needed for trim, hence they are also treated as perturbation variables.

4.5.3 Rig Terms

The forces that are balanced by the rig along the x_{rig} and y_{rig} axes are the sum of the aerodynamic, control and gravitational forces acting on the model, as shown in Figure 6. To determine the components that act along the x_{rig} and y_{rig} axes, the body axes forces are first transformed into rig axes as follows,

$$\begin{bmatrix} \mathbf{X}_{rig} \\ \mathbf{Y}_{rig} \\ 0 \end{bmatrix} = \begin{bmatrix} D_{11} & D_{12} & D_{13} \\ D_{21} & D_{22} & D_{23} \\ D_{31} & D_{32} & D_{33} \end{bmatrix}^{-1} \begin{bmatrix} -\mathbf{X}_{a+c+g} \\ -\mathbf{Y}_{a+c+g} \\ -\mathbf{Z}_{a+c+g} \end{bmatrix}$$

where the subscript $a + c + g$ denotes the sum of aerodynamic, control and gravitational forces. For example, the combined force acting on the model along the x_b axis is given by,

$$\begin{aligned} X_{a+c+g} = & X_{a_e} + \dot{X}_u u + \dot{X}_v v + \dot{X}_w w + \dot{X}_p p + \dot{X}_q q + \dot{X}_r r + \dot{X}_{\dot{w}} \dot{w} + \dot{X}_{\eta} \eta \\ & + \dot{X}_{\xi} \xi + \dot{X}_{\zeta} \zeta + mg\psi \sin \Phi_e \cos \Theta_e - mg\theta \cos \Phi_e \cos \Theta_e \end{aligned} \quad (4.45)$$

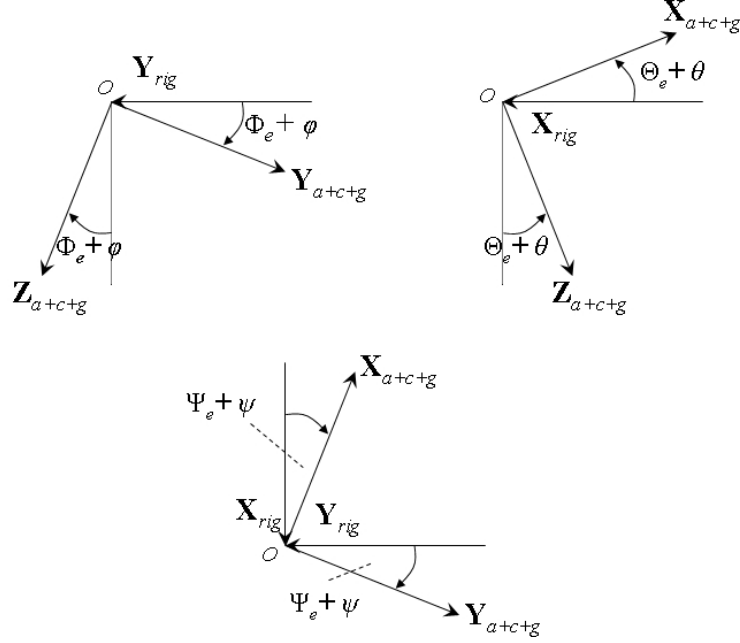


Figure 6: Forces balanced by the rig

Therefore,

$$X_{rig} = -D_{11}X_{a+c+g} - D_{21}Y_{a+c+g} - D_{31}Z_{a+c+g} \quad (4.46)$$

$$Y_{rig} = -D_{12}X_{a+c+g} - D_{22}Y_{a+c+g} - D_{32}Z_{a+c+g} \quad (4.47)$$

These forces can then be transformed back into body axes,

$$\begin{bmatrix} X_{rig_b} \\ Y_{rig_b} \\ Z_{rig_b} \end{bmatrix} = \begin{bmatrix} D_{11} & D_{12} & D_{13} \\ D_{21} & D_{22} & D_{23} \\ D_{31} & D_{32} & D_{33} \end{bmatrix} \begin{bmatrix} X_{rig} \\ Y_{rig} \\ 0 \end{bmatrix} \quad (4.48)$$

$$X_{rig_b} = -(D_{11}^2 + D_{12}^2)X_{a+c+g} - (D_{11}D_{21} + D_{12}D_{22})Y_{a+c+g} - (D_{11}D_{31} + D_{12}D_{32})Z_{a+c+g}$$

$$Y_{rig_b} = -(D_{21}D_{11} + D_{22}D_{12})X_{a+c+g} - (D_{21}^2 + D_{22}^2)Y_{a+c+g} - (D_{21}D_{31} + D_{22}D_{32})Z_{a+c+g}$$

$$Z_{rig_b} = -(D_{31}D_{11} + D_{32}D_{12})X_{a+c+g} - (D_{31}D_{21} + D_{32}D_{22})Y_{a+c+g} - (D_{31}^2 + D_{32}^2)Z_{a+c+g}$$

so, using the expressions for the gravitational, aerodynamic, control and rig terms, the linearised force and moment equations (4.29) to (4.34) can be written as,

$$\begin{aligned} m(\dot{u} - rV_e + qW_e + z_g\dot{q}) = & (1 - (D_{11}^2 + D_{12}^2))X_{a+c+g} \\ & - (D_{11}D_{21} + D_{12}D_{22})Y_{a+c+g} - (D_{11}D_{31} + D_{12}D_{32})Z_{a+c+g} \end{aligned} \quad (4.49)$$

$$\begin{aligned} m(\dot{v} - pW_e + rU_e + \dot{r}x_g - \dot{p}z_g) = & -(D_{21}D_{11} + D_{22}D_{12})X_{a+c+g} \\ & + (1 - (D_{21}^2 + D_{22}^2))Y_{a+c+g} - (D_{21}D_{31} + D_{22}D_{32})Z_{a+c+g} \end{aligned} \quad (4.50)$$

$$m(\dot{w} - qU_e + pV_e - x_g\dot{q}) = -(D_{31}D_{11} + D_{32}D_{12})X_{a+c+g} - (D_{31}D_{21} + D_{32}D_{22})Y_{a+c+g} + (1 - (D_{31}^2 + D_{32}^2))Z_{a+c+g} \quad (4.51)$$

$$I_{xx}\dot{p} - I_{xz}\dot{r} - mz_g(\dot{v} - pW_e + rU_e + \dot{r}x_g - \dot{p}z_g) = L_{a+c+g} \quad (4.52)$$

$$I_{yy}\dot{q} + mz_g(\dot{u} - rV_e + qW_e + z_g\dot{q}) - mx_g(\dot{w} - qU_e + pV_e - \dot{q}x_g) = M_{a+c+g} \quad (4.53)$$

$$I_{zz}\dot{r} - I_{xz}\dot{p} + mx_g(\dot{v} - pW_e + rU_e + \dot{r}x_g - \dot{p}z_g) = N_{a+c+g} \quad (4.54)$$

4.6 Simplification of Equations

It is clear that the expansion of the expressions on the right hand side of Equations (4.49) to (4.54) would lead to some long and very complex terms, particularly for the force equations. To get Equations (4.49) to (4.54) into a more manageable and practical form, some simplifying assumptions can be made.

To start with, it is usual practice for the model to be trimmed with the body xz -plane aligned with the corresponding xz -plane of the rig axes. Therefore the trimmed roll and yaw attitude angles, Φ_e and Ψ_e are zero. Further, if the model is trimmed at a low angle of attack, it may be reasonable to treat Θ_e as a small angle i.e.

$$\cos \Theta_e \approx 1 \text{ and } \sin \Theta_e \approx \Theta_e$$

In this case, the direction cosine matrix for trim reduces to,

$$D_e = \begin{bmatrix} 1 & 0 & -\Theta_e \\ 0 & 1 & 0 \\ \Theta_e & 0 & 1 \end{bmatrix}$$

Hence, the relationship between trimmed velocity components in body axes and rig axes becomes,

$$\begin{bmatrix} U_e \\ V_e \\ W_e \end{bmatrix} = \begin{bmatrix} 1 & 0 & -\Theta_e \\ 0 & 1 & 0 \\ \Theta_e & 0 & 1 \end{bmatrix} \begin{bmatrix} V_T \\ 0 \\ 0 \end{bmatrix} = \begin{bmatrix} V_T \\ 0 \\ V_T\Theta_e \end{bmatrix} \quad (4.55)$$

Following a perturbation from trim, the direction cosine matrix becomes,

$$D = \begin{bmatrix} 1 & \psi & -(\Theta_e + \theta) \\ -\psi & 1 & \phi \\ (\Theta_e + \theta) & -\phi & 1 \end{bmatrix} \quad (4.56)$$

and the body axes velocity components are related to those in rig axes by the expression,

$$\begin{bmatrix} U \\ V \\ W \end{bmatrix} = \begin{bmatrix} U_e + u \\ v \\ W_e + w \end{bmatrix} = \begin{bmatrix} 1 & \psi & -(\Theta_e + \theta) \\ -\psi & 1 & \phi \\ (\Theta_e + \theta) & -\phi & 1 \end{bmatrix} \begin{bmatrix} V_T \\ 0 \\ w_{rig} \end{bmatrix} = \begin{bmatrix} V_T \\ -\psi V_T \\ V_T(\Theta_e + \theta) + w_{rig} \end{bmatrix} \quad (4.57)$$

where products of small perturbations and Θ_e have been assumed to be negligibly small. From Equation (4.57) it can be seen firstly that, under the above assumptions, the perturbation in axial velocity u is zero. Secondly, the trimmed lateral velocity component V_e is also zero. As well as this, the perturbation in yaw angle ψ is equal to the negative perturbation in sideslip angle $-\beta$.

In a similar manner, the body axes angular rate perturbation variables can be expressed in terms of the corresponding rig axes components as,

$$\begin{bmatrix} P \\ Q \\ R \end{bmatrix} = \begin{bmatrix} p \\ q \\ r \end{bmatrix} = \begin{bmatrix} 1 & \psi & -(\Theta_e + \theta) \\ -\psi & 1 & \phi \\ (\Theta_e + \theta) & -\phi & 1 \end{bmatrix} \begin{bmatrix} p_{rig} \\ q_{rig} \\ r_{rig} \end{bmatrix} = \begin{bmatrix} p_{rig} \\ q_{rig} \\ p_{rig} \end{bmatrix} \quad (4.58)$$

where again products of small perturbations and Θ_e have been neglected. Therefore, under the assumptions outlined above, the angular rates in the body axes are equal to their corresponding angular rates in rig axes. Note that the terms describing the disturbance forces and moments can be simplified in a similar manner.

4.6.1 Gravitational Terms

Using the above assumptions, Equations (4.37) and (4.38) can be reduced to,

$$\begin{bmatrix} X_g \\ Y_g \\ Z_g \end{bmatrix} = \begin{bmatrix} -mg(\Theta_e + \theta) \\ mg\phi \\ mg \end{bmatrix} \quad (4.59)$$

$$\begin{bmatrix} L_g \\ M_g \\ N_g \end{bmatrix} = \begin{bmatrix} -x_g mg\psi \\ -x_g mg \\ x_g mg\phi \end{bmatrix} \quad (4.60)$$

4.6.2 Aerodynamic and Control Terms

The aerodynamic and control terms remain largely unchanged from those given in Equations (4.39) to (4.44). However, if it can be assumed that, following a disturbance from trim, the model experiences motion only in the longitudinal plane or the lateral/directional plane then Equations (4.39) to (4.44) can be simplified.

Firstly, for the case in which the model's response to the disturbance is restricted to the longitudinal plane, motion can be completely described by axial force X, normal force Z, pitching moment M, motion variables w , q , θ and elevator input η (remembering that u is assumed to be insignificant). The lateral-directional forces and moments (Y, L, N), motion variables (v , p , r , ϕ , ψ) and control surface inputs (ξ , ζ) are all assumed to be zero. Therefore, derivatives of X, Z and M with respect to lateral-directional variables are negligible and the decoupled longitudinal aerodynamic and control terms can be written as,

$$X_a + X_c = X_{a_e} + \dot{X}_w w + \dot{X}_q q + \dot{X}_{\dot{w}} \dot{w} + \dot{X}_{\eta} \eta \quad (4.61)$$

$$Z_a + Z_c = Z_{a_e} + \dot{Z}_w w + \dot{Z}_q q + \dot{Z}_{\dot{w}} \dot{w} + \dot{Z}_{\eta} \eta \quad (4.62)$$

$$M_a + M_c = M_{a_e} + \dot{M}_w w + \dot{M}_q q + \dot{M}_{\dot{w}} \dot{w} + \dot{M}_{\eta} \eta \quad (4.63)$$

Similarly, the decoupled lateral-directional aerodynamic and control terms can be found by assuming motion due to a disturbance can be characterised completely by lateral force Y, rolling moment L, yawing moment N, motion variables v , p , r , ϕ and ψ and control surface inputs ξ and ζ ,

$$Y_a + Y_c = Y_{a_e} + \dot{Y}_v v + \dot{Y}_p p + \dot{Y}_r r + \dot{Y}_{\xi} \xi + \dot{Y}_{\zeta} \zeta \quad (4.64)$$

$$L_a + L_c = L_{a_e} + \dot{L}_v v + \dot{L}_p p + \dot{L}_r r + \dot{L}_{\xi} \xi + \dot{L}_{\zeta} \zeta \quad (4.65)$$

$$N_a + N_c = N_{a_e} + \dot{N}_v v + \dot{N}_p p + \dot{N}_r r + \dot{N}_{\xi} \xi + \dot{N}_{\zeta} \zeta \quad (4.66)$$

4.6.3 Rig Terms

Again, the forces that are balanced by the rig along the x_{rig} and y_{rig} axes are the sum of the aerodynamic, control and gravitational forces acting on the model and the components that act along the x_{rig} and y_{rig}

axes are found by transforming the body axes into rig axes,

$$\begin{bmatrix} \mathbf{X}_{rig} \\ \mathbf{Y}_{rig} \\ 0 \end{bmatrix} = \begin{bmatrix} 1 & \psi & -(\Theta_e + \theta) \\ -\psi & 1 & \phi \\ (\Theta_e + \theta) & -\phi & 1 \end{bmatrix}^{-1} \begin{bmatrix} -\mathbf{X}_{a+c+g} \\ -\mathbf{Y}_{a+c+g} \\ -\mathbf{Z}_{a+c+g} \end{bmatrix} \quad (4.67)$$

Considering first the longitudinal case, the force along the x_{rig} -axis is found to be,

$$\mathbf{X}_{rig} = -\mathbf{X}_{a+c+g} - \mathbf{Z}_{a+c+g}(\Theta_e + \theta) \quad (4.68)$$

where the longitudinal motion is again assumed to be decoupled from lateral/directional motion, resulting in $\phi = \psi = 0$. Next, for the lateral case, the force along the y_{rig} -axis is,

$$\mathbf{Y}_{rig} = -\mathbf{X}_{a+c+g}\psi - \mathbf{Y}_{a+c+g} - \mathbf{Z}_{a+c+g}\phi \quad (4.69)$$

The expressions for the rig forces given in Equations (4.68) and (4.69) can now be transformed into body axes with the equation,

$$\begin{bmatrix} \mathbf{X}_{rigb} \\ \mathbf{Y}_{rigb} \\ \mathbf{Z}_{rigb} \end{bmatrix} = \begin{bmatrix} 1 & \psi & -(\Theta_e + \theta) \\ -\psi & 1 & \phi \\ (\Theta_e + \theta) & -\phi & 1 \end{bmatrix} \begin{bmatrix} \mathbf{X}_{rig} \\ \mathbf{Y}_{rig} \\ 0 \end{bmatrix} = \begin{bmatrix} -\mathbf{X}_{a+c+g} - \mathbf{Z}_{a+c+g}(\Theta_e + \theta) \\ -\mathbf{Y}_{a+c+g} \\ -\mathbf{X}_{a+c+g}(\Theta_e + \theta) \end{bmatrix} \quad (4.70)$$

and the resulting expressions can be summed with the gravitational, aerodynamic and control terms to give the X, Y and Z force equations,

$$m(qW_e + z_g\dot{q}) = -\mathbf{Z}_{a+c+g}(\Theta_e + \theta) \quad (4.71)$$

$$m(\dot{v} - pW_e + rU_e + \dot{r}x_g - \dot{p}z_g) = 0 \quad (4.72)$$

$$m(\dot{w} - qU_e - x_g\dot{q}) = \mathbf{Z}_{a+c+g} - \mathbf{X}_{a+c+g}(\Theta_e + \theta) \quad (4.73)$$

Note that the \dot{u} term in Equation (4.71) has been dropped as u is assumed to be zero. Expanding the terms \mathbf{X}_{a+c+g} and \mathbf{Z}_{a+c+g} terms, Equations (4.71) to (4.73) become:

$$m(qW_e + z_g\dot{q}) = -(\mathbf{Z}_{a_e} + \dot{\mathbf{Z}}_w w + \dot{\mathbf{Z}}_q q + \dot{\mathbf{Z}}_{\dot{w}} \dot{w} + \dot{\mathbf{Z}}_{\eta} \eta + mg)(\Theta_e + \theta) \quad (4.74)$$

$$m(\dot{v} - pW_e + rU_e + \dot{r}x_g - \dot{p}z_g) = 0 \quad (4.75)$$

$$\begin{aligned} m(\dot{w} - qU_e - x_g\dot{q}) &= \mathbf{Z}_{a_e} + \dot{\mathbf{Z}}_w w + \dot{\mathbf{Z}}_q q + \dot{\mathbf{Z}}_{\dot{w}} \dot{w} + \dot{\mathbf{Z}}_{\eta} \eta + mg \\ &\quad - (\mathbf{X}_{a_e} + \dot{\mathbf{X}}_w w + \dot{\mathbf{X}}_q q + \dot{\mathbf{X}}_{\dot{w}} \dot{w} + \dot{\mathbf{X}}_{\eta} \eta - mg)(\Theta_e + \theta) \end{aligned} \quad (4.76)$$

At trim, by definition, the forces are balanced and all perturbation variables are zero, hence from Equations (4.74) and (4.76),

$$-(\mathbf{Z}_{a_e} + mg)\Theta_e = 0 \quad (4.77)$$

$$\mathbf{Z}_{a_e} + mg - \mathbf{X}_{a_e}\Theta_e = 0 \quad (4.78)$$

and Equations (4.74) to (4.76) can be reduced to:

$$m(qW_e + z_g\dot{q}) = 0 \quad (4.79)$$

$$m(\dot{v} - pW_e + rU_e + \dot{r}x_g - \dot{p}z_g) = 0 \quad (4.80)$$

$$m(\dot{w} - qU_e - x_g\dot{q}) = \dot{\mathbf{Z}}_w w + \dot{\mathbf{Z}}_q q + \dot{\mathbf{Z}}_{\dot{w}} \dot{w} + \dot{\mathbf{Z}}_{\eta} \eta \quad (4.81)$$

where, again, products of perturbations and Θ_e are assumed to be insignificant. The moment equations can be expressed as,

$$\begin{aligned} I_{xx}\dot{p} - I_{xz}\dot{r} - m z_g(\dot{v} - pW_e + rU_e + \dot{r}x_g - \dot{p}z_g) \\ = \mathbf{L}_{a_e} + \dot{\mathbf{L}}_v v + \dot{\mathbf{L}}_p p + \dot{\mathbf{L}}_r r + \dot{\mathbf{L}}_{\xi} \xi + \dot{\mathbf{L}}_{\zeta} \zeta - x_g m g \psi \end{aligned} \quad (4.82)$$

$$\begin{aligned}
I_{yy}\dot{q} + mx_g(qW_e + z_g\dot{q}) - mx_g(\dot{w} - qU_e - \dot{q}x_g) \\
= \overset{\circ}{M}_w w + \overset{\circ}{M}_q q + \overset{\circ}{M}_{\dot{w}} \dot{w} + \overset{\circ}{M}_{\eta} \eta - x_g mg \quad (4.83)
\end{aligned}$$

$$\begin{aligned}
I_{zz}\dot{r} - I_{xz}\dot{p} + mx_g(\dot{v} - pW_e + rU_e + \dot{r}x_g - \dot{p}z_g) \\
= N_{a_e} + \overset{\circ}{N}_v v + \overset{\circ}{N}_p p + \overset{\circ}{N}_r r + \overset{\circ}{N}_{\xi} \xi + \overset{\circ}{N}_{\zeta} \zeta + x_g mg \phi \quad (4.84)
\end{aligned}$$

For the trim case, all moments on the model are balanced and all perturbation variables are zero therefore,

$$L_{a_e} = 0 \quad (4.85)$$

$$M_{a_e} - x_g mg = 0 \quad (4.86)$$

$$N_{a_e} = 0 \quad (4.87)$$

The X and Y force expressions given in Equations (4.79) and (4.80) can also be utilised so that the moment equations become,

$$I_{xx}\dot{p} - I_{xz}\dot{r} = \overset{\circ}{L}_v v + \overset{\circ}{L}_p p + \overset{\circ}{L}_r r + \overset{\circ}{L}_{\xi} \xi + \overset{\circ}{L}_{\zeta} \zeta - x_g mg \psi \quad (4.88)$$

$$I_{yy}\dot{q} - mx_g(\dot{w} - qU_e - x_g\dot{q}) = \overset{\circ}{M}_w w + \overset{\circ}{M}_q q + \overset{\circ}{M}_{\dot{w}} \dot{w} + \overset{\circ}{M}_{\eta} \eta \quad (4.89)$$

$$I_{zz}\dot{r} - I_{xz}\dot{p} = \overset{\circ}{N}_v v + \overset{\circ}{N}_p p + \overset{\circ}{N}_r r + \overset{\circ}{N}_{\xi} \xi + \overset{\circ}{N}_{\zeta} \zeta + x_g mg \phi \quad (4.90)$$

4.7 Equations for 3DoF Case

In practice, it has been found that the wind tunnel models tend to be very responsive in heave, risking damage as they quickly reach the end stops on the vertical rod. One option for dealing with this problem is to implement some form of closed-loop height control system that will prevent the model from reaching the vertical limits. An alternative solution is to completely restrict the motion of the model along the z_{rig} -axis and allow the model to only undergo rotational motion. Consequently the model is constrained to manoeuvre only in 3DoF.

For the 3DoF case, the body axes velocity components are related to the wind tunnel velocity vector by the following expressions,

$$\begin{bmatrix} U \\ V \\ W \end{bmatrix} = \begin{bmatrix} U_e \\ v \\ W_e + w \end{bmatrix} = \begin{bmatrix} 1 & \psi & -(\Theta_e + \theta) \\ -\psi & 1 & \phi \\ (\Theta_e + \theta) & -\phi & 1 \end{bmatrix} \begin{bmatrix} V_T \\ 0 \\ 0 \end{bmatrix} = \begin{bmatrix} V_T \\ -\psi V_T \\ V_T(\Theta_e + \theta) \end{bmatrix} \quad (4.91)$$

The relationship between angular velocities in body axes and those in rig axes remains the same as that given in Equation (4.58).

For the force equations (4.79) to (4.81), the X and Y expressions remain unchanged from the 4DoF case. However, for the Z equation, the aerodynamic, control and gravitational forces are now entirely balanced by the rig hence the right hand side of Equation (4.81) reduces to zero,

$$m(qW_e + z_g\dot{q}) = 0 \quad (4.92)$$

$$m(\dot{v} - pW_e + rU_e + \dot{r}x_g - \dot{p}z_g) = 0 \quad (4.93)$$

$$m(\dot{w} - qU_e - x_g\dot{q}) = 0 \quad (4.94)$$

In terms of the moment equations, the roll and yaw equations are identical to those given in (4.88) and (4.90). For the pitch equation, the Z force component appearing on the left hand side of Equation (4.89)

reduces to zero, hence for the 3DoF case, the moment equations are,

$$I_{xx}\dot{p} - I_{xz}\dot{r} = \dot{L}_v v + \dot{L}_p p + \dot{L}_r r + \dot{L}_\xi \xi + \dot{L}_\zeta \zeta - x_g m g \psi \quad (4.95)$$

$$I_{yy}\dot{q} = \dot{M}_w w + \dot{M}_q q + \dot{M}_{\dot{w}} \dot{w} + \dot{M}_\eta \eta \quad (4.96)$$

$$I_{zz}\dot{r} - I_{xz}\dot{p} = \dot{N}_v v + \dot{N}_p p + \dot{N}_r r + \dot{N}_\xi \xi + \dot{N}_\zeta \zeta + x_g m g \phi \quad (4.97)$$

4.8 State Space Representation

For subsequent analysis, it is convenient to have the equations of motion in state space form. To achieve this, the force and moment equations must first be rearranged so that terms involving state time derivatives appear on the left hand side of the equations, while state variable terms appear on the right hand side. Considering first the longitudinal equations (4.81) and (4.89) for the 4DoF case,

$$(m - \dot{Z}_{\dot{w}})\dot{w} - m x_g \dot{q} = \dot{Z}_w w + (\dot{Z}_q + m U_e) q + \dot{Z}_\eta \eta \quad (4.98)$$

$$-(\dot{M}_{\dot{w}} + m x_g)\dot{w} + (I_{yy} m x_g^2)\dot{q} = \dot{M}_w w + (\dot{M}_q - m x_g U_e) q + \dot{M}_\eta \eta \quad (4.99)$$

The above expressions can be rewritten in the form

$$\mathbf{M}\dot{\mathbf{x}}(t) = \mathbf{A}'\mathbf{x}(t) + \mathbf{B}'\mathbf{u}(t) \quad (4.100)$$

where

$$\mathbf{x}^T(t) = [w \quad q] \quad \mathbf{u}(t) = \eta$$

$$\mathbf{M} = \begin{bmatrix} (m - \dot{Z}_{\dot{w}}) & -m x_g \\ -(\dot{M}_{\dot{w}} + m x_g) & (I_{yy} + m x_g^2) \end{bmatrix} \quad \mathbf{A}' = \begin{bmatrix} \dot{Z}_w & (\dot{Z}_q + m U_e) \\ \dot{M}_w & (\dot{M}_q - m x_g U_e) \end{bmatrix} \quad \mathbf{B}' = \begin{bmatrix} \dot{Z}_\eta \\ \dot{M}_\eta \end{bmatrix}$$

The state space form is obtained by dividing through (4.100) by the mass matrix \mathbf{M} ,

$$\dot{\mathbf{x}}(t) = \mathbf{A}\mathbf{x}(t) + \mathbf{B}\mathbf{u}(t) \quad (4.101)$$

where $\mathbf{A} = \mathbf{M}^{-1}\mathbf{A}'$ and $\mathbf{B} = \mathbf{M}^{-1}\mathbf{B}'$. So the longitudinal state space equations of motion are given by,

$$\begin{bmatrix} \dot{w} \\ \dot{q} \end{bmatrix} = \begin{bmatrix} z_w & z_q \\ m_w & m_q \end{bmatrix} \begin{bmatrix} w \\ q \end{bmatrix} + \begin{bmatrix} z_\eta \\ m_\eta \end{bmatrix} \eta \quad (4.102)$$

The stability and control derivatives appearing in the \mathbf{A} and \mathbf{B} matrices are known as concise derivatives. The definitions for each derivative, for both the 4DoF and 3DoF cases, are given in Appendix A.

The lateral/directional equations are converted in an identical manner to that outlined above for the longitudinal case. Again, using the 4DoF case as an example, Equations (4.80), (4.88) and (4.90) are rearranged to give,

$$m\dot{v} - m z_g \dot{p} + m x_g \dot{r} = m W_e p - m U_e r \quad (4.103)$$

$$I_{xx}\dot{p} - I_{xz}\dot{r} = \dot{L}_v v + \dot{L}_p p + \dot{L}_r r + \dot{L}_\xi \xi + \dot{L}_\zeta \zeta - x_g m g \psi \quad (4.104)$$

$$-I_{xz}\dot{p} + I_{zz}\dot{r} = \dot{N}_v v + \dot{N}_p p + \dot{N}_r r + \dot{N}_\xi \xi + \dot{N}_\zeta \zeta + x_g m g \phi \quad (4.105)$$

With reference to equation (4.100), the state vector \mathbf{x} , control vector \mathbf{u} , mass matrix \mathbf{M} , stability matrix \mathbf{A}' and control matrix \mathbf{B}' for the lateral/directional case are:

$$\mathbf{x}^T(t) = [v \quad p \quad r \quad \phi \quad \psi] \quad \mathbf{u}(t)^T = [\xi \quad \zeta]$$

$$\mathbf{M} = \begin{bmatrix} m & -mz_g & mx_g & 0 & 0 \\ 0 & I_{xx} & -I_{xz} & 0 & 0 \\ 0 & -I_{xz} & I_{zz} & 0 & 0 \\ 0 & 0 & 0 & 1 & 0 \\ 0 & 0 & 0 & 0 & 1 \end{bmatrix} \quad \mathbf{A}' = \begin{bmatrix} 0 & mW_e & -mU_e & 0 & 0 \\ \dot{\mathbf{N}}_v & \dot{\mathbf{N}}_p & \dot{\mathbf{N}}_r & 0 & -x_g mg \\ \mathbf{N}_v & \mathbf{N}_p & \mathbf{N}_r & x_g mg & 0 \\ 0 & 1 & 0 & 0 & 0 \\ 0 & 0 & 1 & 0 & 0 \end{bmatrix} \quad \mathbf{B}' = \begin{bmatrix} 0 & 0 \\ \dot{\mathbf{L}}_\xi & \dot{\mathbf{L}}_\zeta \\ \mathbf{N}_\xi & \mathbf{N}_\zeta \\ 0 & 0 \\ 0 & 0 \end{bmatrix}$$

so the state space lateral/directional equations of motion become:

$$\begin{bmatrix} \dot{v} \\ \dot{p} \\ \dot{r} \\ \dot{\phi} \\ \dot{\psi} \end{bmatrix} = \begin{bmatrix} y_v & y_p & y_r & y_\phi & y_\psi \\ l_v & l_p & l_r & l_\phi & l_\psi \\ n_v & n_p & n_r & n_\phi & n_\psi \\ 0 & 1 & 0 & 0 & 0 \\ 0 & 0 & 1 & 0 & 0 \end{bmatrix} \begin{bmatrix} v \\ p \\ r \\ \phi \\ \psi \end{bmatrix} + \begin{bmatrix} y_\xi & y_\zeta \\ l_\xi & l_\zeta \\ n_\xi & n_\zeta \\ 0 & 0 \\ 0 & 0 \end{bmatrix} \begin{bmatrix} \xi \\ \zeta \end{bmatrix} \quad (4.106)$$

Again, Appendix A contains definitions for each of the concise derivatives in equation (4.106).

5 Experimental Analysis of 1/12 Scale BAe Hawk Data

Having developed the equations of motion from first principles, some experiments were carried out to establish whether these theoretical relationships were valid in practice. The tests were performed on the 1/12 scale BAe Hawk model shown earlier in Figure 1.

An off-the-shelf inertial measurement unit (IMU), shown in Figure 7, was used to record the model motion. The IMU comprised a set of three MEMS accelerometers, three MEMS rate gyros and three solid state magnetometers. The range of these sensors were $\pm 2g$, ± 150 deg/s and ± 2 Gauss respectively. A Kalman filter was used to fuse data from the sensors and provide an accurate measure of the model's Euler angles. The analogue to digital conversion of the measured signals was 16-bit binary and data was sampled from each of the sensors at a maximum rate of 100 Hz. The unit was physically very compact, with dimensions of $5.7 \times 4.5 \times 1.1$ cm and a weight of 33 grams.

Control surface deflections were achieved using miniature servo-actuators (also shown in Figure 7), based on radio controlled aircraft technology. These were physically connected to the relevant control surfaces using standard model control linkages. Commands to the servo-actuators were transmitted from a computer "ground station" through a Bluetooth wireless network. The resultant motion recorded by the sensors was then sent back via the wireless network to the ground station. The use of the Bluetooth network avoided the need to physically connect any cabling to the model, or test rig, thereby eliminating a possible source of interference.

The determination of the equations of motion from experimental data is known as system identification. Figure 8 illustrates the basic principle of the process, which can be applied to both flight test and wind tunnel data. A known input is applied to the aircraft to excite the dynamics of interest and on board sensors are used to measure the aircraft's response. Using this input/output information, a mathematical model of the aircraft dynamics can be constructed.

The major stages involved in the system identification procedure are shown in the block diagram in Figure 9. The first step is the design of the experiments which will be used to excite the aircraft dynamics of interest. This requires some prior knowledge of the vehicle's dynamic characteristics and also includes the selection of appropriate instrumentation to measure the motion variables. Once the data has been recorded, the first stage in the analysis is to verify the consistency of the measurements before they are utilised in later stages of the system identification process. This check on the data, usually termed data compatibility check or flight path reconstruction, is performed by analytically generating the time history

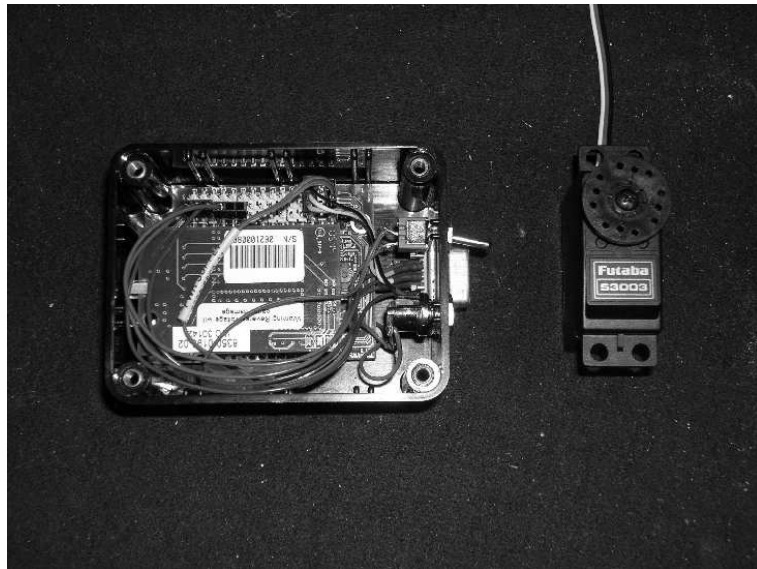


Figure 7: MEMS IMU and miniature servo-actuator

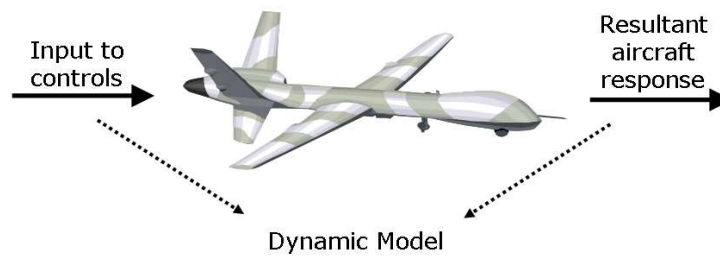


Figure 8: Illustration of system identification

of a given variable using well-defined kinematic relationships and measurements from other variables. For example, the attitude angles can be reconstructed by integrating the rate gyro data. If the measured and reconstructed responses match then the data is said to be kinematically consistent. On the other hand, if the measured and reconstructed responses do not match, error models for each of the sensors can be postulated and the kinematic equations provide a means for estimating these error parameters. Having accounted for errors in the data, the core stage of the analysis is to determine the most appropriate form of the equations to describe the measured response and to estimate the numerical values of the stability and control derivatives appearing in the equations. This is known as model structure determination and parameter estimation respectively. The final step in the analysis is to validate the identified dynamics and this is usually done by comparing the response with a separate set of data not used in the preceding analysis. If the validation process is successful then the analysis is halted and the final model of the aircraft dynamics has been obtained. Otherwise, the analysis may have to be repeated using a different equation structure or parameter estimation technique. In severe cases, the experiments may have to be performed again.

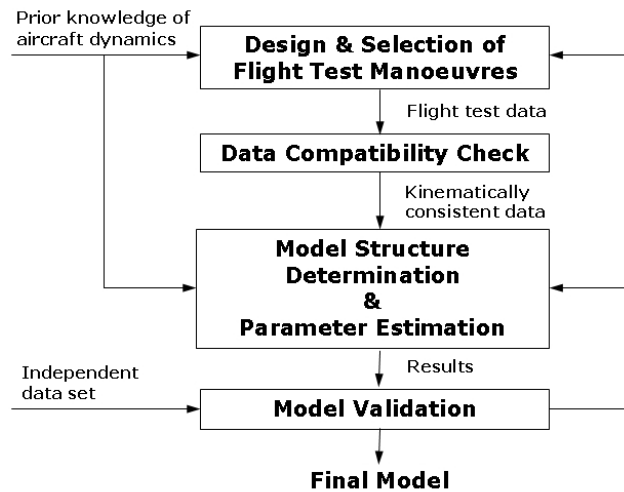


Figure 9: Block diagram of system identification process

This report concentrates on the model structure determination and parameter estimation steps of the analysis. It is therefore assumed that the data compatibility analysis has already been performed on the data.

As well as estimating the model's stability and control derivatives, it was necessary to estimate an equivalent time delay caused principally by the need to transmit and receive data through the wireless network. Accurate knowledge of this time delay was important as it has been shown that time shifts in the data lead to degraded estimates of the stability and control derivatives, particularly if the time shift is in the control input [13]. The block diagram in Figure 10 illustrates the process of transmitting and logging the data. The control inputs were time-logged when the user command was applied at the ground station and the resultant response was time-logged when the data was received from the sensors. Along with the pure time delay introduced by the wireless network, the equivalent time delay parameter also accounts for the phase-lag introduced by unmodelled high-order/high-frequency dynamics. This could include the dynamics of the sensors and associated filters, as well as nonlinearities such as backlash in the control linkages [14]. The state-space equations of motion incorporating a time delay can be written in the general form,

$$\dot{\mathbf{x}}(t) = \mathbf{A}\mathbf{x}(t) + \mathbf{B}\mathbf{u}(t - \boldsymbol{\tau}) \quad (5.1)$$

where $\boldsymbol{\tau}$ is a vector of time delays for each of the control inputs. In general, the state variables contained in the state vector \mathbf{x} may not be measured directly. They are related to the output variables using the

equation,

$$\mathbf{y}(t) = \mathbf{C}\mathbf{x}(t) + \mathbf{D}\mathbf{u}(t - \tau) \quad (5.2)$$

where \mathbf{y} is the output vector containing the variables which are measured during the experiment. The system matrices \mathbf{C} and \mathbf{D} may also contain the stability and control derivatives. In reality, the elements of \mathbf{y} are measured at N discrete points in time,

$$\mathbf{z}(t_k) = \mathbf{y}(t_k) + \boldsymbol{\nu}(t_k) \quad k = 1, 2, \dots, N \quad (5.3)$$

where \mathbf{z} is the measurement vector containing measured values of the elements of \mathbf{y} and $\boldsymbol{\nu}$ is a vector of noise corrupting the measurements of \mathbf{y} . The elements of $\boldsymbol{\nu}$ are assumed to be independent, Gaussian random variables with zero mean.

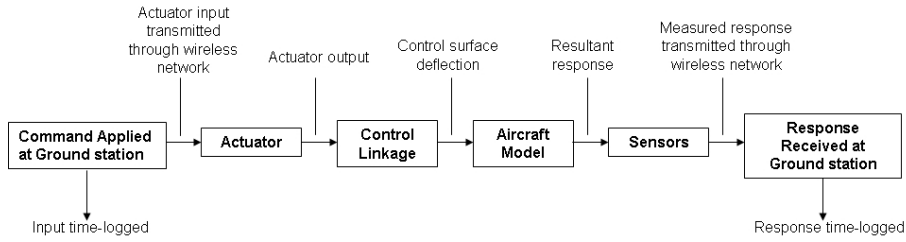


Figure 10: Transmission and logging of data

The choice was made to perform the analysis in the frequency domain, which is better suited to the estimation of time delays than time domain approaches. As the data is sampled at discrete time points, time domain estimates of τ have to be integer multiples of the data sampling time Δt , unless the data is interpolated before hand. For the frequency domain, as the analysis is performed at discrete frequencies rather than discrete time points, the elements of τ are identified directly as real numbers regardless of the value of Δt . A second reason for adopting a frequency domain approach was the observation of an undesirable structural vibration in the rig during the tests. This can be seen in Figure 11, which shows a plot of the Fourier sine series coefficients of the angle of attack data against frequency. The Fourier sine series coefficients with large amplitudes located at frequencies below 3Hz belong to the model's rigid body dynamics. Above 3Hz, the amplitudes reduce to a relatively small and constant value, which corresponds to noise in the data. However, the amplitudes increase again at approximately 8-9Hz. This is caused by the structural vibration. By performing parameter estimation in the frequency domain, the analysis can be restricted to a given band of frequencies and, thus, the rigid body dynamics can be isolated from the higher frequency structural vibration.

The experimental data was transformed into the frequency domain using a chirp-z Fourier transform, which allows the frequencies of interest to be specified arbitrarily [15]. The lower frequency limit (in Hertz) was chosen as $2/T$, where T is the duration of the manoeuvre under analysis. This meant that, for each frequency, there was at least two full sinusoidal waveforms. The upper limit was selected so that the model dynamics of interest were included in the frequency band and was typically chosen as 3Hz. A resolution of 0.02Hz was used.

The parameter estimates were obtained using the equation error method. For the state space system given by Equations (5.1) and (5.2), the aim of the equation error approach is to find a model which matches the time derivatives of the states $\dot{\mathbf{x}}$ derived from the measured data.

In the frequency domain, Equations (5.1) to (5.3) become

$$j\omega_k \tilde{\mathbf{x}}(\omega_k) = \mathbf{A}\tilde{\mathbf{x}}(\omega_k) + \mathbf{B}\tilde{\mathbf{u}}(\omega_k)e^{-j\omega_k\tau} \quad (5.4)$$

$$\tilde{\mathbf{y}}(\omega_k) = \mathbf{C}\tilde{\mathbf{x}}(\omega_k) + \mathbf{D}\tilde{\mathbf{u}}(\omega_k)e^{-j\omega_k\tau} \quad (5.5)$$

$$\tilde{\mathbf{z}}(\omega_k) = \tilde{\mathbf{y}}(\omega_k) + \tilde{\boldsymbol{\nu}}(\omega_k) \quad k = 1, 2, \dots, N \quad (5.6)$$

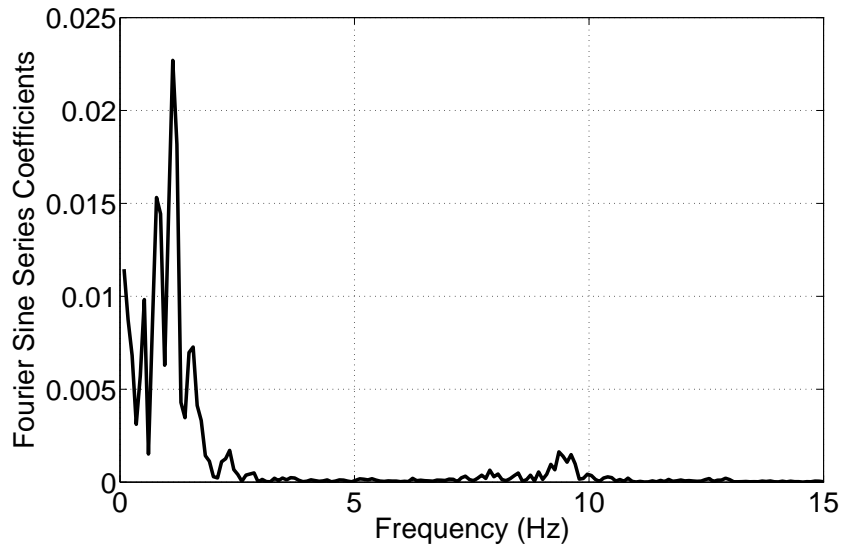


Figure 11: Fourier sine series coefficients of the angle of attack signal against frequency

where $\tilde{\cdot}$ denotes a variable transformed into the frequency domain and ω_k is the vector of N discrete frequencies in rad/s. The equivalent time delay term makes the parameter estimation problem a nonlinear one, hence it was not possible to solve the equation error problem using linear regression. Instead, the modified Newton-Raphson technique, normally applied in the output error formulation, was used for the equation error method. As this algorithm is iterative, it required specification of initial values for the unknown parameters, unlike linear regression which is a one-shot method. However, the equation error method is robust to starting values of the parameters [15] and it was found that the initial estimates could all be set to zero without affecting convergence.

A detailed mathematical description of the modified Newton-Raphson technique and its application in frequency domain estimation is not given here. The interested reader can find this material covered in Klein and Morelli [15]. A brief summary of the important relationships in the algorithm, however, is given below. The cost function to be minimized is

$$J(\gamma) = N \sum_{k=1}^N \tilde{\mathbf{v}}^\dagger(\omega_k, \gamma) \mathbf{S}_{\nu\nu}^{-1} \tilde{\mathbf{v}}(\omega_k, \gamma) + N \ln |\mathbf{S}_{\nu\nu}| \quad (5.7)$$

where $\mathbf{S}_{\nu\nu}$ is a real diagonal matrix whose elements are the power spectral densities of the elements of ν and the symbol \dagger denotes the complex conjugate transpose. The vector γ contains the unknown parameters to be determined. In the formulation of the equation error method, the state derivatives are treated as measured values; $\tilde{\mathbf{y}}(\omega_k)$ in Equation (5.6) is replaced by $j\omega_k \tilde{\mathbf{x}}(\omega_k)$ and the equation errors, or innovations, are defined as

$$\tilde{\mathbf{v}}(\omega_k) = \tilde{\mathbf{z}}(\omega_k) - \mathbf{A}\tilde{\mathbf{x}}(\omega_k) + \mathbf{B}\tilde{\mathbf{u}}(\omega_k) \quad (5.8)$$

Estimates of the power spectral density matrix are obtained from

$$\hat{\mathbf{S}}_{\nu\nu} = \sum_{k=1}^N \tilde{\mathbf{v}}^\dagger(\omega_k, \hat{\gamma}) \tilde{\mathbf{v}}(\omega_k, \hat{\gamma}) \quad (5.9)$$

where $\hat{\cdot}$ is used to denote an estimated vector and the vector of parameter estimates for the i th iteration is calculated from,

$$\hat{\gamma}_i = \hat{\gamma}_{i-1} + \Delta\gamma \quad (5.10)$$

The parameter update is given by

$$\Delta\boldsymbol{\gamma} = - \left[\frac{\partial^2 J(\boldsymbol{\gamma})}{\partial\boldsymbol{\gamma}\partial\boldsymbol{\gamma}^T} \right]^T \left[\frac{\partial J(\boldsymbol{\gamma})}{\partial\boldsymbol{\gamma}} \right] \quad (5.11)$$

Convergence is achieved and the process is halted when the relative change in the cost function and/or the update to the parameter estimates from one iteration to the next falls below a user-defined threshold.

In Equation (5.11), the second-order gradient of the the cost function with respect to the parameter vector is known as the Fisher information, or Hessian, matrix. It indicates the curvature of the cost function to variations in each of the unknown parameters and is an important factor in determining the accuracy of the parameter estimates. The statistical accuracy of the parameter estimates on the basis of the Cramer-Rao inequality. This can be written as,

$$\text{Cov}(\hat{\boldsymbol{\gamma}}) \geq \left[\frac{\partial^2 J(\boldsymbol{\gamma})}{\partial\boldsymbol{\gamma}\partial\boldsymbol{\gamma}^T} \right]^{-1} \quad (5.12)$$

In other words, the information matrix gives a theoretical minimum for the achievable parameter covariance. An exact solution for the information is difficult to obtain in practice. For the modified Newton-Raphson algorithm, it is calculated approximately from,

$$\mathbf{H} \approx \frac{\partial^2 J(\boldsymbol{\gamma})}{\partial\boldsymbol{\gamma}\partial\boldsymbol{\gamma}^T} \approx 2N\text{Re} \left[\sum_{k=0}^{N-1} \frac{\partial\tilde{\boldsymbol{\nu}}^\dagger(\omega_k)}{\partial\boldsymbol{\gamma}} \hat{\mathbf{S}}_{\boldsymbol{\nu}\boldsymbol{\nu}} \frac{\partial\tilde{\boldsymbol{\nu}}(\omega_k)}{\partial\boldsymbol{\gamma}} \right] \quad (5.13)$$

where the difficult to compute second-order partial derivatives of $\tilde{\boldsymbol{\nu}}$ with respect to $\boldsymbol{\gamma}$ have been neglected. The validity of this approximation improves the closer the parameter estimates get to the real derivative values.

From the Cramer-Rao inequality, three important statistical metrics of the parameter estimates can be calculated. Firstly, the Cramer-Rao bound of the i th parameter estimate is defined as,

$$\text{CR}_i = \sqrt{(\mathbf{H}^{-1})_{ii}} \quad i = 1, \dots, n_\gamma \quad (5.14)$$

where n_γ is the number of unknown parameters. The Cramer-Rao bound provides a measure of the minimum expected standard deviation of the parameter that would be obtained from analysis of repeated manoeuvres.

In practice, the Cramer-Rao bound under predicts the scatter of parameters estimates for repeated manoeuvres, particularly when the estimation is performed in the time domain. This is due to the fact that in the development of the estimation algorithms, the innovations $\boldsymbol{\nu}$ are assumed to be characterised by Gaussian, white noise. This means that the power of the noise is evenly distributed across the frequency range $[0, f_N]$ where $f_N = 1/2\Delta t$ is the Nyquist frequency. In reality, innovations are coloured as the noise power is concentrated within a particular frequency band. For aircraft parameter estimation, this occurs in the frequency band corresponding to the rigid body dynamics [15]. Coloured innovations is due to errors in the model specification and the noise on the measured variables themselves being coloured. From experience, the Cramer-Rao bounds obtained from time domain estimates can be around 5 to 10 times smaller than the corresponding standard deviations [16]. In the frequency domain, however, the analysis is restricted to the frequencies in which the rigid body dynamics are situated. Despite the noise being coloured, the power of the noise in this low frequency band is relatively constant. Therefore, the assumptions made about the noise in the development of the algorithm match more closely in practice when the analysis is performed in the frequency domain rather than in the time domain. In turn, the Cramer-Rao bounds obtained from frequency domain estimation should match more closely to the standard deviations. However, it has been found that a factor of 2 is still needed [14, 16]. So for the i th parameter estimate, the standard deviation is given approximately by,

$$\sigma_i \approx 2\text{CR}_i = 2\sqrt{(\mathbf{H}^{-1})_{ii}} \quad (5.15)$$

The second statistical metric is parameter insensitivity, which for the i th parameter is given by,

$$I_i = \frac{1}{\sqrt{\mathbf{H}_{ii}}} \quad (5.16)$$

The insensitivity is a measure of how much a parameter value can be changed without causing an increase in the cost function. It therefore provides a measure of the significance of each parameter and can be used to determine the most appropriate form of the equations of motion for a given response.

It is convenient to express both the Cramer-Rao bound and insensitivity as a percentage of the identified parameter value,

$$\overline{\text{CR}}_i = \left| \frac{\text{CR}_i}{\gamma_i} \right| \times 100 \quad (5.17)$$

$$\overline{I}_i = \left| \frac{I_i}{\gamma_i} \right| \times 100 \quad (5.18)$$

At first glance, it may appear from Equations (5.14) and (5.16) that the Cramer-Rao bound and insensitivity are the same. However, there is a subtle difference between the two. The insensitivity is approximately the conditional standard deviation of the parameter estimate, given that all other parameters are known. The Cramer-Rao bound is an approximation of the unconditional standard deviation [16].

The third metric is the pair-wise correlation between the i th and the j th parameters which is defined as,

$$\rho_{ij} = \frac{\mathbf{H}_{ij}^{-1}}{\sqrt{\mathbf{H}_{ii}^{-1}\mathbf{H}_{jj}^{-1}}} \quad i, j = 1, \dots, n_\gamma \quad (5.19)$$

The absolute value of ρ_{ij} (for $i \neq j$) falls between 0 and 1. If $\rho_{ij} = 1$, then the i th and j th parameters are linearly dependent and are both accounting for the same effect in the model describing the aircraft's response. This means that accurate estimates for both derivatives cannot be obtained, as many weighted combinations of the two parameters could be used equally well to fit the measured motion. The solution is to hold one of the parameters fixed at some appropriate value and estimate the other derivative as normal. In practice, because of measurement errors, it is rare to find $\rho_{ij} = 1$ but correlation coefficients greater than 0.9 can indicate near-linear dependency between the two derivatives and should be investigated further [15, 17].

A major drawback of pair-wise correlation analysis is that it can only be used reliably to indicate correlation between two parameters. It may not show linear dependence between three or more parameters. An example of where correlation between multiple parameters can occur is in aircraft requiring stability augmentation. If more than one motion variable is being fed back to the control surface as part of the control law, then those motion variables and the control input will all be linearly dependent in some way. A method of detecting correlation between multiple parameters is the uncertainty or confidence ellipsoid [14, 16]. For the i th parameter with Cramer-Rao bound CR_i , this can be expressed as [14],

$$\overline{\Theta}_{\text{CR}_i} = \frac{\mathbf{T}^{-1}\mathbf{H}^{-1}(:, i)}{\text{CR}_i} \quad (5.20)$$

where \mathbf{T} is a diagonal matrix containing the sensitivities from Equation (5.16) and $\mathbf{H}^{-1}(:, i)$ denotes the i th column of the inverse of the information matrix. Correlation is indicated if any of the elements of $\overline{\Theta}_{\text{CR}_i}$ are relatively big in comparison to the element corresponding to the i th parameter.

An approach to model structure determination based on the statistical metrics described above is outlined by Tischler [14]. The Cramer-Rao bounds and insensitivities are both assigned threshold values. The aim of the process is to obtain a set of equations for which all the derivatives meet these limits and therefore have a roughly constant degree of confidence. Initially, parameter estimation is carried out with all possible parameters included in the model structure. The insensitivities are checked against the

threshold and derivative with the highest insensitivity exceeding the limit is removed from the analysis by being set to zero or some other appropriate a-priori value and parameter estimation is repeated. This process continues until all derivatives remaining in the model structure have insensitivities within the threshold. At this stage, it may be that all derivatives have acceptable insensitivities but the Cramer-Rao bounds of some parameters are large. This is most likely due to correlation between parameters, so the confidence ellipsoid for the parameter with the biggest Cramer-Rao bound is analysed. If linear dependence between parameters is indicated then a choice of which parameter to drop must be made. This decision can be a difficult one and it may be useful to rely on an understanding of the physics of the aircraft to choose which derivative to remove from the model structure. At each step in the process, the value of the cost function is also analysed. If a significant increase in the cost function occurs as a result of removing a parameter from the model then that parameter is re-entered into the equations and the current model is acceptable as the final model structure.

Suggested guidelines for satisfactory parameter estimates are $\bar{C}R_i \leq 20\%$ (with CR_i calculated from Equation (5.15)) and $\bar{I}_i \leq 10\%$ [14]. However, it should be noted that these thresholds are suggested for the case where the cost function is expressed in terms of frequency response curves, separated into magnitude and phase components. The errors between the measured and predicted response is weighted according to the coherence at each discrete frequency. Coherence is a measure of the linearity between the input and output data. The difference in the formulation of the cost function for the frequency response case and that given in Equation (5.7) means that the definition of the information matrix for the two methods also differs. Therefore, the limits of $\bar{C}R_i \leq 20\%$ and $\bar{I}_i \leq 10\%$ may not be reliable guidelines for the equation error method. However, the Cramer-Rao bound, insensitivity, pair-wise correlation and confidence ellipsoid make no assumptions about which estimation technique is being used, so an attempt to carry out a model structure determination analysis, similar to that described above (but using the equation error method), on data obtained from the 4DoF facility was made. The goal of the process was to obtain a model structure in which the parameters all had Cramer-Rao bounds and insensitivities of similar magnitudes.

It is worth noting that other approaches to the aircraft model structure determination process exist, most notably the modified stepwise regression technique [15, 18]. However, as already pointed out, the need to account for the time delay τ means that this particular case cannot be formulated as a regression problem. Hence, the method described above is viewed as the most appropriate for the current application.

5.1 Longitudinal Example

For the tests on the Hawk model, heaving motion was restrained so only 3DoF motion was allowed. The input used to excite the dynamics was a 0.3s 1-1-2 multistep input to the elevator [19] (see Figure 12). The wind tunnel velocity, V_T , was 30m/s, with the model trimmed at an angle of attack $\alpha_e = 0^\circ$, resulting in $\Theta_e = W_e = 0$. The Hawk's centre of gravity was also coincident with the location of the gimbal, therefore $x_g = z_g = 0$. Using the derivative definitions in Appendix A, for the given conditions the normal force derivatives z_w and z_η should theoretically be zero and $z_q = U_e = V_T$. Therefore, the theoretical state equation can be expressed as,

$$\begin{bmatrix} \dot{w}(t) \\ \dot{q}(t) \end{bmatrix} = \begin{bmatrix} 0 & z_q \\ m_w & m_q \end{bmatrix} \begin{bmatrix} w(t) \\ q(t) \end{bmatrix} + \begin{bmatrix} 0 \\ m_\eta \end{bmatrix} \eta(t - \tau_\eta) \quad (5.21)$$

where τ_η is the time delay on the elevator input. While pitch rate q is measured directly, the normal velocity w is derived from angle of attack/pitch attitude data. So the output equation for this case is,

$$\begin{bmatrix} \alpha(t) \\ q(t) \end{bmatrix} = \begin{bmatrix} 1/V_T & 0 \\ 0 & 1 \end{bmatrix} \begin{bmatrix} w(t) \\ q(t) \end{bmatrix} + \begin{bmatrix} 0 \\ 0 \end{bmatrix} \eta(t - \tau_\eta) \quad (5.22)$$

Table 4 contains theoretical estimates of the derivatives in Equation (5.21) from empirical analysis of the Hawk model [1], therefore a comparison between theoretical and the experimental derivatives can be made.

Parameter	Estimate
z_w	0
z_q	30
z_η	0
m_w	-1.64
m_q	-4.01
m_η	-2.60
τ_η	-

Table 4: Empirical estimates of derivatives

For the analysis of the experimental data, all derivatives are initially treated as free parameters to be estimates so the starting state equation is,

$$\begin{bmatrix} \dot{w}(t) \\ \dot{q}(t) \end{bmatrix} = \begin{bmatrix} z_w & z_q \\ m_w & m_q \end{bmatrix} \begin{bmatrix} w(t) \\ q(t) \end{bmatrix} + \begin{bmatrix} m_w \\ m_\eta \end{bmatrix} \eta(t - \tau_\eta) \quad (5.23)$$

Table 5 shows the initial parameter estimates for the model structure given by Equation (5.23). Two parameters, z_w and z_η , stand out having both large Cramer-Rao bounds and high insensitivity factors in relation to the other derivatives. The Cramer-Rao bounds of z_w and z_η are around two orders of magnitude greater than those for the other parameters, while the insensitivities are an order of magnitude larger in comparison. With the highest insensitivity of 89.53%, the choice is made to repeat the parameter estimation process with z_w removed from the model by holding its value at zero. The results of the second parameter estimation analysis are shown in Table 6. In comparison to the initial estimates given in Table 5, the values of the parameters retained in the model have remained almost constant. At the same time, the cost function value has also remained virtually unchanged, with a slight decrease from $J = 123.27$ to $J = 122.94$. The fact that the parameter estimates and the cost function are largely unaffected by the removal of z_w from the model structure validates the choice of fixing this parameter at zero. Focusing on the remaining terms in the equations of motion, again z_η has a significantly larger Cramer-Rao bound and insensitivity when compared to the other derivatives. Therefore, for the third parameter estimation step z_η is also held at a fixed value of zero.

Par.	$\hat{\gamma}$	$\bar{C}R\%$	$\bar{I}\%$
z_w	0.035	189.60	89.53
z_q	28.583	1.40	0.47
z_η	-0.096	165.75	55.68
m_w	-1.552	4.73	1.79
m_q	-3.805	10.54	3.14
m_η	-2.114	6.97	2.25
τ_η	0.253	2.93	1.03
$J = 123.27$			

Table 5: Initial parameter estimates

Par.	$\hat{\gamma}$	$\bar{C}R\%$	$\bar{I}\%$
z_w	0.000	-	-
z_q	28.566	1.40	0.47
z_η	-0.103	155.65	52.33
m_w	-1.552	4.71	1.80
m_q	-3.851	10.15	3.11
m_η	-2.122	6.96	2.25
τ_η	0.253	2.92	1.02
$J = 122.94$			

Table 6: Parameter estimates - z_w dropped

Table 7 shows the results of removing z_η from the model. Again, the parameter estimates are largely unaffected by fixing z_η at zero and, in fact, the Cramer-Rao bounds of some of the derivatives have dropped. The cost function has also reduced slightly from $J = 122.94$ to $J = 122.57$. Hence, it can again be concluded that a more appropriate model structure to describe the measured response has been

obtained by removing z_η from the analysis. Note that the Cramer-Rao bounds and insensitivities of the remaining parameters are all now of similar magnitudes.

Par.	$\hat{\gamma}$	$\bar{C}R \%$	$\bar{I} \%$
z_w	0.000	-	-
z_q	28.719	0.99	0.47
z_η	0.000	-	-
m_w	-1.553	4.72	1.81
m_q	-3.968	9.97	3.05
m_η	-2.173	6.88	2.22
τ_η	0.255	2.74	1.00
$J = 122.57$			

Table 7: Parameter estimates - z_η dropped

Having removed z_η from the model, the structure obtained from the experimental data is the same as that predicted from theory (see Equation (5.21)). Also, comparison of the derivative values in Table 7 with those in Table 4 indicate a very close match between the empirical and experimental estimates, which match to within 5%. Consequently the choice was made to halt the identification at this point. Figure 12 shows the time histories of w and q derived from the measured data against the responses reconstructed from the identified model. Also shown is the elevator input used to excite the longitudinal dynamics.

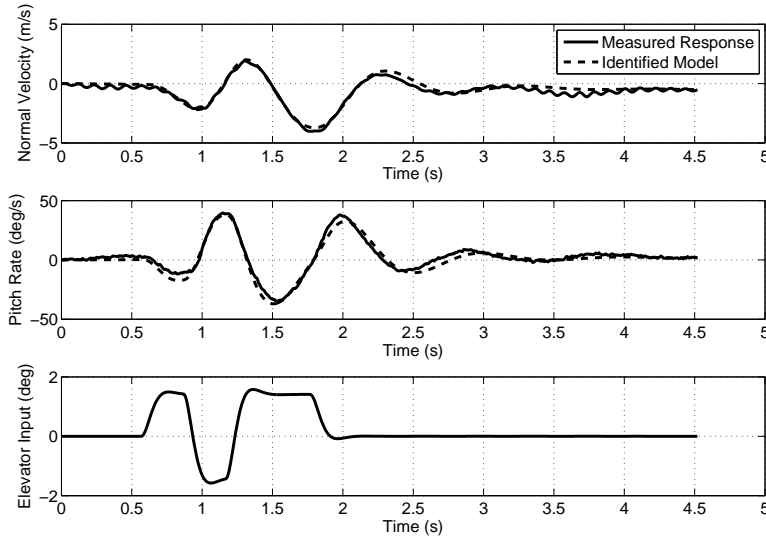


Figure 12: Comparison of measured and identified responses for final model structure

5.2 Lateral/Directional Example

For this example, the tests on the Hawk were carried out at the same conditions as for the longitudinal case described in Section 5.1. The rudder input for the experiment was a 1-1-2 multistep input of similar duration [19] (see Figure 13). The wind tunnel velocity was $V_T=30\text{m/s}$, with the model trimmed at angle of attack $\alpha_e = 0\text{deg}$, resulting in $\Theta_e = W_e = 0$. The Hawk's centre of gravity was also coincident with the location of the gimbal, therefore $x_g = z_g = 0$.

For the data analysed in this example, a control input to excite the dynamics was applied to the rudder

only so the identification of the derivatives due to aileron deflection ξ cannot be identified from these particular measurements. From Appendix A, the derivatives with respect to roll attitude ϕ and yaw attitude ψ should also be zero, as $x_g = z_g = 0$. For the same reason, the theoretical values of lateral force derivatives are $y_v = y_p = y_\zeta = 0$ and $y_r = -U_e = -V_T$. Under these assumptions, the lateral/directional equations of motion given reduce to,

$$\begin{bmatrix} \dot{v}(t) \\ \dot{p}(t) \\ \dot{r}(t) \end{bmatrix} = \begin{bmatrix} 0 & 0 & y_r \\ l_v & l_p & l_r \\ n_v & n_p & n_r \end{bmatrix} \begin{bmatrix} v(t) \\ p(t) \\ r(t) \end{bmatrix} + \begin{bmatrix} 0 \\ l_\zeta \\ n_\zeta \end{bmatrix} \zeta(t - \tau_\zeta) \quad (5.24)$$

where τ_ζ is the time delay on the rudder input. The roll rate p and the yaw rate r are measured directly but the sideslip velocity v is obtained from angle of sideslip/yaw attitude data. The output equation in this case is,

$$\begin{bmatrix} \beta(t) \\ p(t) \\ r(t) \end{bmatrix} = \begin{bmatrix} 1/V_T & 0 & 0 \\ 0 & 1 & 0 \\ 0 & 0 & 1 \end{bmatrix} \begin{bmatrix} v(t) \\ p(t) \\ r(t) \end{bmatrix} + \begin{bmatrix} 0 \\ 0 \\ 0 \end{bmatrix} \zeta(t - \tau_\zeta) \quad (5.25)$$

It may be reasonable to assume that the rolling motion caused by the rudder input will be insignificant in comparison to the yawing motion. In this case, the roll equation and derivatives with respect to p can be removed from Equation (5.24) giving,

$$\begin{bmatrix} \dot{v} \\ \dot{r} \end{bmatrix} = \begin{bmatrix} 0 & y_r \\ n_v & n_r \end{bmatrix} \begin{bmatrix} v \\ r \end{bmatrix} + \begin{bmatrix} 0 \\ n_\zeta \end{bmatrix} \zeta \quad (5.26)$$

Empirically derived estimates [1] for the parameters in Equation (5.26) are shown in Table 8, again allowing a comparison with experimental estimates.

Parameter	Estimate
y_v	0
y_r	-30
y_ζ	0
n_v	1.28
n_r	-1.53
n_ζ	-0.67
τ_ζ	-

Table 8: Empirical estimates of derivatives

For the parameter estimation analysis, the initial model structure was taken to be,

$$\begin{bmatrix} \dot{v}(t) \\ \dot{p}(t) \\ \dot{r}(t) \end{bmatrix} = \begin{bmatrix} y_v & y_p & y_r \\ l_v & l_p & l_r \\ n_v & n_p & n_r \end{bmatrix} \begin{bmatrix} v(t) \\ p(t) \\ r(t) \end{bmatrix} + \begin{bmatrix} y_\zeta \\ l_\zeta \\ n_\zeta \end{bmatrix} \zeta(t - \tau_\zeta) \quad (5.27)$$

As some rolling motion following the rudder input was observed when the tests were carried out the roll equation and derivatives with respect to p are included in the initial model. Table 9 shows the results for the initial parameter estimation analysis. The derivative y_ζ clearly stood out as having the highest insensitivity. Therefore, it was removed from the model and the analysis was repeated. This was done a number of times with the successive removal of the derivatives l_r, l_ζ, l_p and l_v (results shown in Tables 10 to 14). At this stage of the process, the analysis had indicated that there was insufficient information in the data to reliably identify any of the rolling moment derivatives. However, y_p and n_p were still

candidate terms for the model structure, therefore p was dropped as a state variable and instead treated as a pseudo input [17]. Hence the equations of motion were rearranged to give,

$$\begin{bmatrix} \dot{v}(t) \\ \dot{r}(t) \end{bmatrix} = \begin{bmatrix} y_v & y_r \\ n_v & n_r \end{bmatrix} \begin{bmatrix} v(t) \\ r(t) \end{bmatrix} + \begin{bmatrix} 0 & y_p \\ n_\zeta & n_p \end{bmatrix} \begin{bmatrix} \zeta(t - \tau_\zeta) \\ p(t) \end{bmatrix} \quad (5.28)$$

Comparison of Tables 13 and 14 shows that, when the model structure was rearranged as above, the cost function value dropped significantly.

Par.	$\hat{\gamma}$	$\bar{C}R$ %	\bar{I} %
y_v	0.057	86.27	29.28
y_p	0.981	60.02	19.08
y_r	-29.943	0.87	0.30
y_ζ	0.001	7645.70	2541.16
l_v	0.187	82.21	27.04
l_p	-1.199	151.03	47.41
l_r	-0.438	187.18	62.82
l_ζ	0.098	193.11	62.05
n_v	0.955	3.51	1.15
n_p	-0.876	44.96	14.08
n_r	-1.375	14.05	4.35
n_ζ	-0.603	6.69	2.18
τ_ζ	0.262	2.35	0.95
$J = 170.75$			

Table 9: Initial parameter estimates

Par.	$\hat{\gamma}$	$\bar{C}R$ %	\bar{I} %
y_v	0.063	64.91	26.41
y_p	0.877	53.54	21.24
y_r	-29.924	0.64	0.30
y_ζ	0.000	-	-
l_v	0.224	61.18	22.63
l_p	-1.708	87.55	33.37
l_r	0.000	-	-
l_ζ	0.168	82.75	36.20
n_v	0.958	3.41	1.15
n_p	-0.884	44.43	13.97
n_r	-1.389	13.91	4.31
n_ζ	-0.605	6.69	2.18
τ_ζ	0.262	2.30	0.95
$J = 169.22$			

Table 11: Parameter estimates - l_r dropped

Par.	$\hat{\gamma}$	$\bar{C}R$ %	\bar{I} %
y_v	0.059	69.16	28.13
y_p	0.927	50.81	20.14
y_r	-29.938	0.64	0.30
y_ζ	0.000	-	-
l_v	0.189	81.34	26.79
l_p	-1.199	150.74	47.39
l_r	-0.427	191.50	64.41
l_ζ	0.102	183.98	59.48
n_v	0.955	3.51	1.15
n_p	-0.875	44.99	14.09
n_r	-1.376	14.05	4.34
n_ζ	-0.603	6.70	2.18
τ_ζ	0.262	2.33	0.95
$J = 170.76$			

Table 10: Parameter estimates - y_ζ dropped

Par.	$\hat{\gamma}$	$\bar{C}R$ %	\bar{I} %
y_v	0.066	61.86	25.16
y_p	0.899	52.23	20.73
y_r	-29.912	0.64	0.30
y_ζ	0.000	-	-
l_v	0.164	79.49	31.33
l_p	-1.067	133.43	54.20
l_r	0.000	-	-
l_ζ	0.000	-	-
n_v	0.960	3.42	1.15
n_p	-0.806	48.71	15.37
n_r	-1.402	13.80	4.28
n_ζ	-0.604	6.66	2.19
τ_ζ	0.261	2.26	0.96
$J = 174.32$			

Table 12: Parameter estimates - l_ζ dropped

The next two parameters to be removed from the model structure were y_p , followed by y_v (Tables 15 and 16). When this was carried out, it can be seen from Table 16 that the insensitivities of the remaining parameters were all of a similar magnitude. However, the Cramer-Rao bound of n_p was high in comparison to the other derivatives. As described above, a parameter with high Cramer-Rao bound but low insensitivity could be an indication of correlation among the derivatives. Therefore, the confidence ellipsoid for n_p was examined, See Table 17 (note that the elements have been scaled to unity). The table

indicates that the high Cramer-Rao bound for n_p may have been high due to some correlation with n_v , n_r and n_ζ , although the values are moderate. To investigate further, parameter estimation was repeated one more time with n_p eliminated from the model. The results are shown in Table 18.

Par.	$\hat{\gamma}$	$\bar{\text{CR}} \%$	$\bar{\text{I}} \%$
y_v	0.068	59.93	24.39
y_p	0.811	57.44	22.88
y_r	-29.893	0.63	0.30
y_ζ	0.000	-	-
l_v	0.112	98.51	46.52
l_p	0.000	-	-
l_r	0.000	-	-
l_ζ	0.000	-	-
n_v	0.966	3.38	1.14
n_p	-0.885	44.27	13.99
n_r	-1.393	13.86	4.31
n_ζ	-0.601	6.69	2.20
τ_ζ	0.262	2.26	0.96
$J = 172.63$			

Table 13: Parameter estimates - l_p dropped

Par.	$\hat{\gamma}$	$\bar{\text{CR}} \%$	$\bar{\text{I}} \%$
y_v	0.074	54.89	22.51
y_p	0.568	82.80	32.93
y_r	-29.891	0.64	0.30
y_ζ	0.000	-	-
l_v	0.000	-	-
l_p	0.000	-	-
l_r	0.000	-	-
l_ζ	0.000	-	-
n_v	0.981	3.35	1.14
n_p	-1.490	26.55	8.40
n_r	-1.237	15.35	4.90
n_ζ	-0.583	6.92	2.29
τ_ζ	0.259	2.37	1.01
$J = 100.93$			

Table 14: Parameter estimates - l_v dropped
(p set as a pseudo input)

With n_p removed, the model structure matched that predicted from theory. The estimates of the derivatives in Table 18 also matched closely to the empirical values given in Table 8. The agreement between experimental and empirical estimates was not as good when n_p was included in the model structure. As well as this, without n_p in the equations, the Cramer-Rao bounds of most of the remaining parameters fell, particularly for n_r . However, the cost function increased slightly with the removal of the parameter. Figure 13 shows the time histories of v and r derived from the measured data against the responses reconstructed from the identified model. Reconstructed responses with and without n_p are shown and it can be seen that, visually at least, there is very little difference between the two identified responses. It is therefore a borderline decision as to whether n_p should remain in the model. However, on balance, it is probably appropriate to eliminate n_p from the final model. This decision could be based simply on the principle of parsimony which says that given two models which have similar levels of fidelity, the better model is that which has the fewer number of parameters [17].

5.3 Comments on the Experimental Results

In both the examples described above, the model structure determination procedure was found to work well, with the final models derived from the wind tunnel data matching the equations of motion predicted from theory. This may be unsurprising considering the approach used was originally developed for rotorcraft applications [14], in which the equations of motion can be far more complex than those outlined in this report. It is also worth noting that, despite using a different parameter estimation technique, the suggested guidelines of $\bar{\text{CR}}_i \leq 20\%$ and $\bar{\text{I}}_i \leq 10\%$ have worked well for the two examples. It is clear, however, that the process of model structure determination is one that cannot be used blindly but instead works best when utilised in conjunction with a physical understanding of the aircraft dynamics. This is especially true in cases where the statistical metrics give conflicting advice on whether or not a parameter should be retained in the equations of motion.

Par.	$\hat{\gamma}$	$\bar{\text{CR}} \%$	$\bar{\text{I}} \%$
y_v	0.102	33.66	16.78
y_p	0.000	-	-
y_r	-29.827	0.63	0.31
y_ζ	0.000	-	-
l_v	0.000	-	-
l_p	0.000	-	-
l_r	0.000	-	-
l_ζ	0.000	-	-
n_v	0.979	3.35	1.14
n_p	-1.457	27.16	8.60
n_r	-1.238	15.35	4.90
n_ζ	-0.582	6.94	2.29
τ_ζ	0.259	2.38	1.01
$J = 100.36$			

Table 15: Parameter estimates - y_p dropped

Par.	$\hat{\gamma}$	$\bar{\text{CR}} \%$	$\bar{\text{I}} \%$
y_v	0.000	-	-
y_p	0.000	-	-
y_r	-29.817	0.70	0.35
y_ζ	0.000	-	-
l_v	0.000	-	-
l_p	0.000	-	-
l_r	0.000	-	-
l_ζ	0.000	-	-
n_v	0.984	3.33	1.13
n_p	-1.459	27.15	8.60
n_r	-1.252	15.19	4.85
n_ζ	-0.582	6.95	2.30
τ_ζ	0.259	2.38	1.01
$J = 100.06$			

Table 16: Parameter estimates - y_v dropped

Parameter	$\bar{\Theta}_{\text{CR}_{n_p}}$
y_r	0.001
n_v	-0.633
n_p	1.000
n_r	-0.572
n_ζ	-0.584
τ_ζ	0.112

Table 17: Confidence ellipsoid elements for n_p dropped

6 Conclusions

The equations of motion of an aircraft model tested in Cranfield's 4 degree-of-freedom (DoF) dynamic wind tunnel have been developed. In previous research, the equations have been derived assuming that the model's centre of gravity (cg) is coincident with the gimbal mechanism about which the model rotates on the rig. However, in this report, a general approach was taken with the cg assumed to be located away from the gimbal. The equations were developed from first principles and reduced to a linearised form where motion can be represented as small perturbations about trim. The equations were also decoupled into longitudinal and lateral/direction expressions and converted into state space form. It had been found in practice that models tested in the facility were very responsive in heave and could only be operated open-loop if movement was restricted to purely rotational motion. Therefore, the equations for this 3DoF case were also developed. Having obtained theoretical expressions for the equations of motion, a series of wind tunnel tests were conducted on a 1/12 scale BAe Hawk model in order to establish if the theoretical relations were valid in practice. The particular technique used in testing the model was dynamic simulation and the analysis of the experimental data was performed using system identification. An established model structure determination procedure was used to determine which stability and control derivatives should be included in the equations of motion. Frequency domain equation error parameter estimation was then used to obtain numerical values for the stability and control derivatives. For both the longitudinal and lateral/directional examples described, the final model structure obtained from experiment matched that derived from theory. Derivatives values obtained from parameter estimation and empirical analysis were also in good agreement.

Par.	$\hat{\gamma}$	$\bar{C}R$ %	\bar{I} %
y_v	0.000	-	-
y_p	0.000	-	-
y_r	-29.812	0.71	0.35
y_ζ	0.000	-	-
l_v	0.000	-	-
l_p	0.000	-	-
l_r	0.000	-	-
l_ζ	0.000	-	-
n_v	0.912	3.13	1.44
n_p	0.000	-	-
n_r	-1.682	11.06	4.26
n_ζ	-0.672	5.68	2.34
τ_ζ	0.264	2.36	1.01
$J = 101.53$			

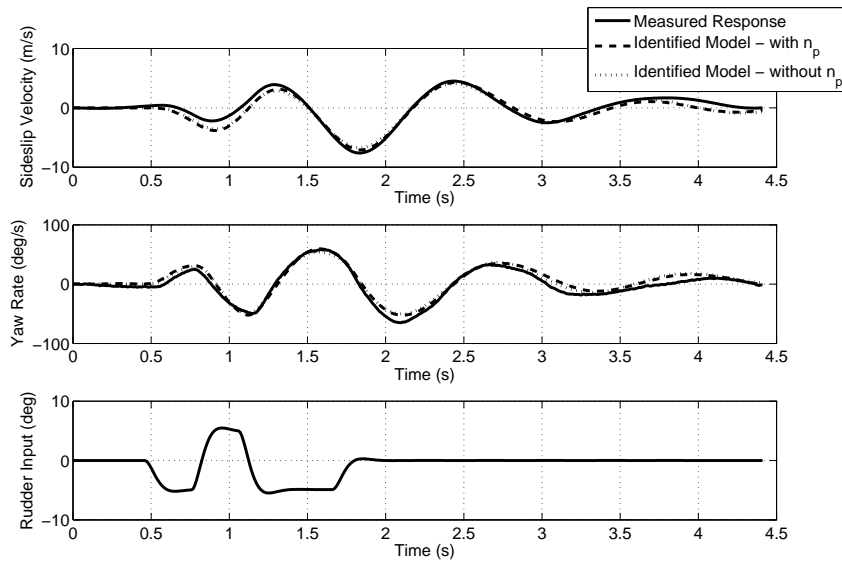
Table 18: Parameter estimates - n_p dropped

Figure 13: Comparison of measured and identified responses for final model structure

References

- [1] Malik, I. A. "The design, development and evaluation of an active control aircraft model wind tunnel facility". PhD thesis, College of Aeronautics, Cranfield Institute of Technology, 1982.
- [2] Kumar, H. "A preliminary study into the design of a free flight wind tunnel model for demonstrating the dynamic characteristics of aircraft". Master's thesis, College of Aeronautics, Cranfield Institute of Technology, 1980.
- [3] Heydari, F. "On the estimation of stability and control characteristics of a generalised forward swept wing aircraft". PhD thesis, College of Aeronautics, Cranfield Institute of Technology, 1986.
- [4] Hinds, H. A. "The application of a modified stepwise regression (MSR) method to the estimation of aircraft stability and control derivatives". PhD thesis, College of Aeronautics, Cranfield Institute of Technology, 1996.
- [5] Barlow, J. B., Rae, W. H. and Pope, A. *Low-speed Wind Tunnel Testing*. John Wiley, New York, 3rd edition, 1999.
- [6] Anderson, J. D. *Fundamentals of Aerodynamics*. McGraw-Hill, Boston, 3rd edition, 2001.
- [7] Cook, M. V. On the use of small scale aircraft models for dynamic wind tunnel investigation of stability and control. *Transactions of the Institute of Measurement and Control*. Vol. 9, No. 4, 1987, pp 190 - 197.
- [8] Bennett, R. M., Farmer, M. G., Mohr, R. L., and Hall, E. W. Wind tunnel technique for determination of dynamic stability derivatives from cable-mounted models. *Journal of Aircraft*. Vol. 15, No. 5, 1978, pp 304-309.
- [9] Subke, H. Test installations to investigate the dynamic behaviour of aircraft with scaled models in wind tunnels. *Transactions of the Institute of Measurement and Control*. Vol. 1, No. 3, 1979, pp 135 - 140.
- [10] B. Krag. The wind tunnel behaviour of a scaled model with a gust alleviation system in a deterministic gust field. *Transactions of the Institute of Measurement and Control*. Vol. 1, No. 3, 1979, pp 141 - 153.
- [11] M. S. Rajamurthy. Generation of comprehensive longitudinal aerodynamic data using dynamic wind-tunnel simulation. *Journal of Aircraft*. Vol. 34, No.1, 1997, pp 29 - 33.
- [12] Cook, M.V. *Flight Dynamics Principles*. Edward Arnold, London, 1997.
- [13] Steers, S. T., and Iliff, K. W. Effects of time-shifted data on flight-determined stability and control derivatives. NASA-TN-D-7830, March 1975.
- [14] Tischler, M. B., and Remple, R. K. *Aircraft and Rotorcraft System Identification: Engineering Methods with Flight Test Examples*. American Institute of Aeronautics and Astronautics, Reston, Virginia, 2006.
- [15] Klein, V., and Morelli, E. A. *Aircraft System Identification: Theory and Practice*. American Institute of Aeronautics and Astronautics, Reston, Virginia, 2006.
- [16] Maine, R.E. and Iliff, K.W. The theory and practice of estimating the accuracy of dynamic flight-determined coefficients. NASA Reference Publication 1077, 1981.
- [17] Jategaonkar, Ravindra V. *Flight Vehicle System Identification: A Time Domain Methodology*. American Institute of Aeronautics and Astronautics, Reston, Virginia, 2006.

- [18] Klein, V., Batterson, J.G. and Murphy, P.C. Determination of airplane model structure from flight data by using modified stepwise regression. NASA Technical Paper 1916, 1981.
- [19] Carnduff, S. D., Erbsloeh, S. D., Cooke, A. K. and Cook, M. V. Development of a low cost dynamic wind tunnel facility utilizing mems inertial sensors. *46th AIAA Aerospace Sciences Meeting & Exhibit*, Reno, Nevada, 2008.

A Definition of Concise Derivatives

A.1 Longitudinal Derivatives

A.1.1 4DoF Case

The denominator for each of the derivatives is given by:

$$(I_{yy} + mx_g^2)(m - \dot{Z}_{\dot{w}}) - mx_g^2(\dot{M}_{\dot{w}} + mx_g) \quad (\text{A.1})$$

while each of the numerators can be expressed as follows,

$$z_w : \dot{Z}_w(I_{yy} + mx_g^2) + mx_g\dot{M}_w \quad (\text{A.2})$$

$$z_q : (\dot{Z}_q + mU_e)(I_{yy} + mx_g^2) + (\dot{M}_q - mx_gU_e)mx_g \quad (\text{A.3})$$

$$z_\eta : \dot{Z}_\eta(I_{yy} + mx_g^2) + \dot{M}_\eta mx_g \quad (\text{A.4})$$

$$m_w : \dot{Z}_w(\dot{M}_{\dot{w}} + mx_g) + \dot{M}_w(m - \dot{Z}_{\dot{w}}) \quad (\text{A.5})$$

$$m_q : (\dot{Z}_q + mU_e)(\dot{M}_{\dot{w}} + mx_g) + (\dot{M}_q - mx_gU_e)(m - \dot{Z}_{\dot{w}}) \quad (\text{A.6})$$

$$m_\eta : \dot{Z}_\eta(\dot{M}_{\dot{w}} + mx_g) + \dot{M}_\eta(m - \dot{Z}_{\dot{w}}) \quad (\text{A.7})$$

A.1.2 3DoF Case

The denominator for each of the derivatives is given by:

$$m(I_{yy} + mx_g^2) - mx_g^2(\dot{M}_{\dot{w}} + mx_g) \quad (\text{A.8})$$

while each of the numerators can be expressed as follows,

$$z_w : mx_g\dot{M}_w \quad (\text{A.9})$$

$$z_q : mU_e(I_{yy} + mx_g^2) + (\dot{M}_q - mx_gU_e)mx_g \quad (\text{A.10})$$

$$z_\eta : \dot{M}_\eta mx_g \quad (\text{A.11})$$

$$m_w : m\dot{M}_w \quad (\text{A.12})$$

$$m_q : mU_e(\dot{M}_{\dot{w}} + mx_g) + m(\dot{M}_q - mx_gU_e) \quad (\text{A.13})$$

$$m_\eta : m\dot{M}_\eta \quad (\text{A.14})$$

A.2 Lateral/Directional Derivatives

Note that the lateral/directional derivatives given in this section are the same for both the 4DoF and 3DoF cases. The denominator for each of the derivatives is given by:

$$m(I_{xx}I_{zz} - I_{xz}^2) \quad (\text{A.15})$$

while each of the numerators can be expressed as follows,

$$y_v : \dot{L}_v(I_{xx}mz_g - I_{xz}mx_g) + \dot{N}_v(I_{xz}mz_g - I_{xx}mx_g) \quad (\text{A.16})$$

$$y_p : mW_e(I_{xx}I_{zz} - I_{xz}^2) + \dot{L}_p(I_{xx}mz_g - I_{xz}mx_g) + \dot{N}_p(I_{xz}mz_g - I_{xx}mx_g) \quad (\text{A.17})$$

$$y_r : -mU_e(I_{xx}I_{zz} - I_{xz}^2) + \dot{L}_r(I_{xx}mz_g - I_{xz}mx_g) + \dot{N}_r(I_{xz}mz_g - I_{xx}mx_g) \quad (\text{A.18})$$

$$y_\phi : x_g mg(I_{xz}mz_g - I_{xx}mx_g) \quad (\text{A.19})$$

$$y_\psi : -x_g mg(I_{zz}mz_g - I_{xz}mx_g) \quad (\text{A.20})$$

$$y_\xi : \dot{L}_\xi(I_{xx}mz_g - I_{xz}mx_g) + \dot{N}_\xi(I_{xz}mz_g - I_{xx}mx_g) \quad (\text{A.21})$$

$$y_\zeta : \dot{L}_\zeta(I_{xx}mz_g - I_{xz}mx_g) + \dot{N}_\zeta(I_{xz}mz_g - I_{xx}mx_g) \quad (\text{A.22})$$

$$l_v : \dot{L}_v m I_{zz} + \dot{N}_v m I_{xz} \quad (\text{A.23})$$

$$l_p : \dot{L}_p m I_{zz} + \dot{L}_p m I_{xz} \quad (\text{A.24})$$

$$l_r : \dot{L}_r m I_{zz} + \dot{N}_r m I_{xz} \quad (\text{A.25})$$

$$l_\phi : x_g m^2 g I_{xz} \quad (\text{A.26})$$

$$l_\psi : -x_g m^2 g I_{zz} \quad (\text{A.27})$$

$$l_\xi : \dot{L}_\xi m I_{zz} + \dot{N}_\xi m I_{xz} \quad (\text{A.28})$$

$$l_\zeta : \dot{L}_\zeta m I_{zz} + \dot{N}_\zeta m I_{xz} \quad (\text{A.29})$$

$$n_v : \dot{L}_v m I_{xz} + \dot{N}_v m I_{xx} \quad (\text{A.30})$$

$$n_p : \dot{L}_p m I_{xz} + \dot{N}_p m I_{xx} \quad (\text{A.31})$$

$$n_r : \dot{L}_v m I_{xz} + \dot{N}_r m I_{xx} \quad (\text{A.32})$$

$$n_\phi : x_g m^2 g I_{xx} \quad (\text{A.33})$$

$$n_\psi : -x_g m^2 g I_{xz} \quad (\text{A.34})$$

$$n_\xi : \dot{L}_\xi m I_{xz} + \dot{N}_\xi m I_{xx} \quad (\text{A.35})$$

$$n_\zeta : \dot{L}_\zeta m I_{xz} + \dot{N}_\zeta m I_{xx} \quad (\text{A.36})$$